Computational modelling and microfluidics as emerging approaches to synthesis of silver nanoparticles – a review

Nathanael, Konstantia; Pico, Paula; Kovalchuk, Nina M.; Lavino, Alessio D.; Simmons, Mark J.H.; Matar, Omar K.

DOI:
10.1016/j.cej.2022.135178

Document Version
Peer reviewed version

Citation for published version (Harvard):
Nathanael, K, Pico, P, Kovalchuk, NM, Lavino, AD, Simmons, MJH & Matar, OK 2022, 'Computational modelling and microfluidics as emerging approaches to synthesis of silver nanoparticles – a review', *Chemical Engineering Journal*, vol. 436, 135178. https://doi.org/10.1016/j.cej.2022.135178

Computational modelling and microfluidics as emerging approaches to synthesis of silver nanoparticles – A review

Konstantia Nathanael[1], Paula Pico[2*], Nina M. Kovalchuk[1], Alessio D. Lavino[2], Mark J. H. Simmons[1], Omar K. Matar[2]

[1]School of Chemical Engineering, University of Birmingham, B15 2TT, UK

[2]Department of Chemical Engineering, Imperial College London, London, SW7 2AZ, UK

*Corresponding Author's email: p.pico20@imperial.ac.uk

*Corresponding Author's telephone: +44 7593782927

Abstract

This review provides an integrated overview of the current state of knowledge for sustainable production of silver nanoparticles (AgNPs), focussing on recent advances in their synthesis using emerging microfluidic-based methods and computational modelling, their properties and practical applications. Special attention is given to the Finke-Watzky two-step kinetic model, which provides the best fitting for nucleation and growth of AgNPs and the multiple operating parameters that affect their physical and chemical properties. An overview of numerical simulations used to model the synthesis of AgNPs across different length and time scales is presented. Investigations made at the molecular scale via molecular dynamics (MD) simulations, at the meso- and macroscale via population balance modelling (PBM) and computational fluid dynamics (CFD), respectively are discussed, alongside data-driven modelling approaches. The review also identifies both limitations and advantages in exploiting the aforementioned techniques, offering a way forward for further investigations on the topic. A critical analysis of the literature leads to confirm that the combination of microfluidics-based

synthesis, which enable reactions to be carried out under highly-controlled conditions, along with physics-driven simulations and data-driven models are a powerful tool to effectively link input information of the process and output data related to the properties of the AgNPs. This combined framework therefore provides an opportunity to improve the prediction accuracy of the whole cycle of synthesis of AgNPs and overcome the environmental impact and limitations of traditional methods.

Keywords: *Sustainable synthesis; microfluidic synthesis; silver nanoparticles; computational modelling; data-driven models.*

Highlights:

- Microfluidic synthesis methods allow better control the formation process of AgNPs.
- MD, PBM and CFD are promising tools to analyse the underlying physics of AgNPs.
- Data-driven models can help link operating conditions to final properties of AgNPs.
- Pairing experiments, data-driven and physics-based models for sustainable synthesis.

Table of Contents

1.Introduction

According to the Allied Market Research report released in 2020 [1], the global market of silver nanoparticles (AgNPs) was valued at $1.8 million in 2019 and it is projected to reach $4.1 billion by 2027. During this forecast period, it is expected that the application of AgNPs in the pharmaceutical sector will increase at the fastest growth rate in terms of volume and revenue due to their antibacterial and antiviral activity. AgNPs possess some unique properties which have enabled their application in multiple areas, as shown in **Figure 1.**

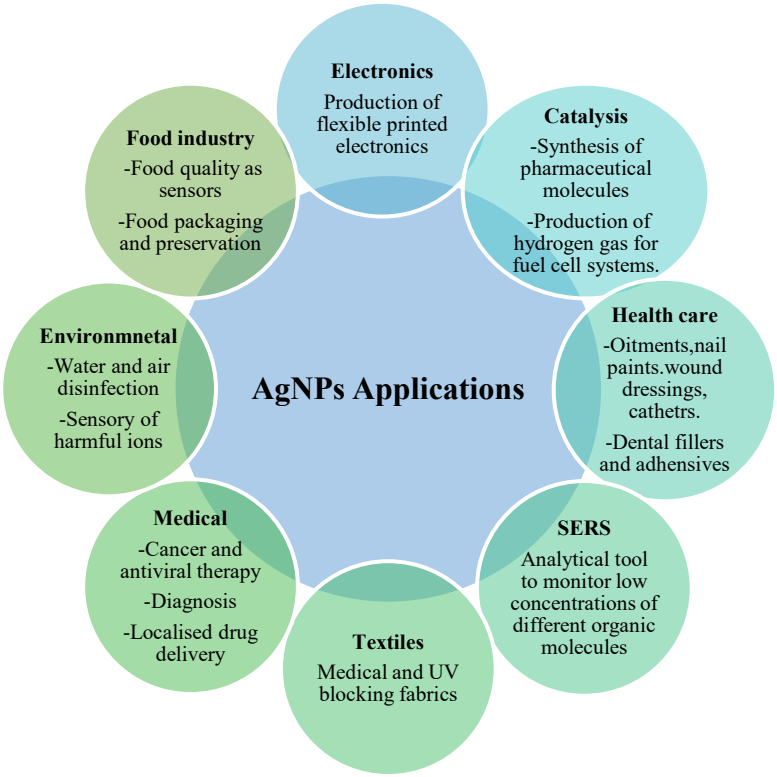

Figure1: Summary of the main applications of AgNPs

AgNPs are effective against many bacteria including some antibiotic-resistant strains [2] and viruses [3], [4]. The enhanced antibacterial properties of silver at the nanoscale are valuable for applications in filters for water disinfection [5], food packaging and preservation [6], sterile textiles [7], the health care sector as skin products [8], wound dressings [9], catheters [10], and dental materials [9]. In skin products, these nanoparticles are employed as cleansers to kill harmful bacteria and treat acne or seborrheic dermatitis [8]. AgNPs can also be embedded into finger and toenail paints to treat fungal infections [11] or incorporated in textile fabrics to contribute in the production of antibacterial clothing for hospitals and laboratories [12]. Other medical applications of AgNPs include diagnostics and bioimaging [13], drug delivery systems [14], and cancer treatment [15].

Silver is the most electrically conductive element. For nanoparticles, the melting temperature decreases with size as a result of increased surface energy. Thus, coalescence and sintering of nanoparticles within a deposited film can be chemically induced at room temperature, resulting in a highly conductive thin silver film [16]. For this reason, conductive inks and silver films are among the most used materials in

the development of printed and flexible electronics [17]. A notably important application of the silver-based inks is in the production of electrochemical sensors to detect ions or determine compounds such as paracetamol in biological and pharmaceutical samples [18],[19].

AgNP-catalysts are highly effective given their large surface area to volume ratio and high selectivity. They find applications for general organic reactions [20] and degradation of various organic dyes, including 4-nitrophenol (4-NP), methylene blue (MB), methyl orange (MO), phenol red (PR), and direct blue (DB24) [21]. AgNPs are also very promising catalysts for the production of hydrogen for fuel cells [22]. When electromagnetic radiation interacts with AgNPs, it induces a collective oscillation of surface conduction electrons called surface plasmons. Existence of surface plasmons during their interaction with light are also responsible for the strong interaction of Ag colloids in UV-Vis spectral region [23]. This allows the application of AgNPs in colorimetric probes for the selective sensing of different molecules in the food industry [24], water quality control [25], and medical diagnostics [26]. The plasmonic properties of AgNPs can be also used in surface-enhanced Raman scattering (SERS) [27]. SERS is a sensitive and effective spectroscopic technique to monitor trace amounts of different organic molecules, such as adenine [28] and tartrazine [29].

The properties of various nanoparticles, including AgNPs, are largely dependent on their size and shape, which in turn are influenced by the fabrication method. There are various routes for AgNPs synthesis which can be divided into top-down and bottom-up methods. Top-down processes start from the bulk material and decrease the size of the particles to the desired values. Bottom-up methods use atomic, molecular, or ionic components to generate the more complex nanoscale structures [30]. Top-down approaches mainly utilise physical methods [31] while bottom-up routes exploit different chemical [32], physical [33], and biological [34] processes. Recent and comprehensive reviews of the various physical, chemical and biological available methods for the synthesis of AgNPs are described by Zahoor, Nazir [35] and Yaqoob, Umar [36]. The fabrication of AgNPs via chemical methods, which comprise most of this review, is specifically characterised by the nature of the reactants used. A growing list of viable chemicals for synthesis has been developing over the past few years aiming for an effective, cheap, and environmentally-friendly production.

Traditional approaches to research and development of new processes of AgNPs fabrication have often relied on 'trial and error' paths, large-scale batch-style chemical reactors, and 'one-at-a-time' experimental runs. Despite the simplicity of these approaches, their systematic adoption has some considerable disadvantages, such as excessive energy and material consumption, waste production, poor parameter control, substantial variation in quality between different samples, as well as low reproducibility [37]. It is therefore necessary to develop methods that enable a sustainable and controlled AgNPs synthesis route to reduce the ecological footprint and overcome the limitations of traditional methods. This review focuses on two approaches that have emerged in the past few years and have gained significant attention from both academia and industry. The first approach is concerned with AgNPs synthesis via microfluidics, which enables chemical reactions to be carried out under highly-controlled conditions with low reactants consumption and high rates of mass and heat transfer. The second approach consists of computational simulations of various levels of fidelity, which have provided information regarding the most effective synthesis route and the most influential operating parameters on the final properties of AgNPs. They have also allowed understanding of the underlying physical phenomena that take part during production. The combination of these approaches could be a promising path to increase the sustainability of AgNPs production.

This manuscript is intended to provide an overview of the most significant advances made for the synthesis of AgNPs and of their properties from an experimental and computational perspective, placing particular focus on microfluidic systems and highlighting potential areas for future research. The review begins with a discussion of the chemical synthesis methods and reactants found in the literature in §2. §3 is mostly dedicated to Finke-Watzky model [38] for nucleation and growth of NPs, which provides the best fitting for reaction kinetics as compared with other models, such as the LaMer model [39] and Ostwald ripening [40]. The role of various operating parameters on the final properties of AgNPs, with emphasis on the importance of monodispersity for multiple applications is discussed in §4. Recent developments in the use of multiscale computational modelling to predict the behaviour of the reacting system during synthesis and the final properties of AgNPs, as well as understanding of their molecular interactions with a third component are given in §5. §6 is devoted to microfluidic drop and continuous-

flow reactors, their use in AgNPs synthesis, and related numerical approaches used to simulate these systems. Conclusions and an overview of future perspectives in the field are given in §7.

2.Chemical synthesis of AgNPs

Various approaches for the chemical synthesis of AgNPs are found in the literature, including photochemical [41] and electrochemical [42] techniques. Photochemical techniques use electromagnetic radiation to influence chemical reactions, while electrochemical techniques utilise electricity to force the movement of electrons causing chemical changes. Chemical reduction is one of the most common approaches to produce AgNPs as it requires simple equipment, which allows for large-scale production [32]. Thermal decomposition of different silver precursors, such as silver acetate [43] and silver oxalate [44] is another possible way to produce AgNPs. The chemical reduction may occur in solid-state [45] and in a flow of inert gas such as N_2 [43].

Reactions are usually carried out in macroscale reactors, but microreactors employing microfluidics or microemulsions, are of growing interest. A microemulsion is a thermodynamically stable dispersion of surfactants, oil, and water [46] where the droplets are of 10-100 nm in size and can act as reactors to perform chemical reactions. Specifically in aqueous droplets, silver salts are reduced to generate AgNPs. Different surfactants can be used for the microemulsion technique, such as sodium dodecyl sulphate (SDS) [47], cetyltrimethylammonium bromide (CTAB), and Triton X-100 [46]. Using microfluidics in the fabrication of AgNPs is addressed in detail in §6.

Chemical reduction consists of three steps that are described mathematically in the next section: the reduction of silver ions (Ag^+) to silver atoms (Ag^0) using reducing agents such as borohydrides [48], hydrazine compounds [49], polyols [50], and sugars [51], nucleation and stabilisation of growing particles using surfactants like CTAB [52], or polymers like poly(vinylpyrrolidone) (PVP) [50] and poly (ethylene glycol) (PEG) [42]. Thiols [53] and citrates [54] are also widely used as stabilizers in the synthesis of AgNPs. Homogenous nucleation takes place when a nucleus begins to form within a parent phase. This process can be described thermodynamically by the total free energy of a NP, which

is determined as the sum of the surface free energy and the volume free energy. As the surface free energy is always positive and the volume energy is always negative, there is a maximum free energy where a stable nucleus with a given critical radius can be formed. The critical radius is the minimum size of a nucleus which can be formed in a solution without being redissolved. In general, the formed nuclei then serve as templates for crystal growth to give colloidal AgNPs with varied diameters [55]. The use of stabilising or capping agents, which adsorb or bind onto the surfaces of the NPs, prevents the further growth and aggregation of NPs and make the colloidal system kinetically stable [56].

Borohydrides [48], boranes [57], hydrazine hydrate [49] and aniline [52] are examples of strong reducing agents while ethylene glycol [50], glycose [51] and tannic acid [58] are weak reducing agents [59]. Silver salts, including $AgClO_4$ [60],[61] , $AgCF_3COO$ [62], $AgNO_3$ [63], $AgCH_3COO$ [64],[65] or $(PPh_3)_n$ Ag-R (R= Cl, Br or NO_3 and n=1 or 3) [66] can be used as silver precursors. However, silver nitrate is the most common precursor due to its low cost and chemical stability [67]. Examples of AgNPs synthesized using different chemical methods with different precursors and reducing agents are presented in **Table 1.** The reducing agents in **Table 1** have been organised in an order of decreasing reducing strength.

Green chemistry has received a lot of attention in recent years in line with the increasing demands of more environmentally friendly, non-toxic, and clean approaches to the production of AgNPs and other materials. The use of toxic chemicals and solvents can be avoided using reducing and capping agents generated by plant systems, such as *Melia dubia* [68], *Melia azedarach* [68] or fruit extracts and fruit peels such as *Sterculia acuminata* [21]. For instance, *C. camphora* [69], *Lippia citriodora* [70] coffee and tea extracts [71] have been used to synthesize AgNPs as they contain alkaloids, flavonoids and carbohydrate compounds, which have been reported as reducing agents [72]. Examples of green chemistry methods are provided also in **Table 1.**

1

Table 1: Examples of chemical synthesis methods of AgNPs.

Method	Silver precursor	Reducing agent	Stabilising agent or surfactant	Particle size (nm)	Particle Shape	Activity/Application	References
Chemical reduction	$AgNO_3$	$NaBH_4$	Dodecanoic acid (DDA)	appr.7 nm	Spherical	Application as electrodes in printed circuit boards.	[48]
Chemical reduction	$AgNO_3$	$NaBH_4$	PVP	9.0 ± 2.1 nm	Spherical	Application as building blocks for the fabrication of NPs-based thin films.	[49]
Chemical reduction	$AgCH_3COO$	$NaBH_4$	PVP	Not stated.	Not stated.	The prepared AgNPs functionalized with 4-ATP were combined with Fe_3O_4 NPs in order to apply in biomedicine.	[65]
Chemical reduction	$AgNO_3$	$NaBH_4$	Trisodium citrate	Appr.9.94 nm	Spherical and hemispherical	Antimicrobial activity against *Staphylococcus aureus*, *Escherichia coli*, *Escherichia coli* AmpC	[32]

						resistant and *Candida albicans.*	
Chemical reduction(micro emulsion)	$AgNO_3$	$NaBH_4$	Triton X-100	appr. 8 nm	Disc shaped	Antimicrobial activity against *Escherichia coli* and *Candida albicans.*	[46]
Chemical reduction	$AgClO_4$	$NaBH_4$	Without any stabilizing agent.	Radius 5-8 nm. 20-30 % polydispersity.	Spherical	Not stated.	[73]
Chemical reduction	$AgClO_4$	$NaBH_4$	PVP	Radius 5-7 nm. 15-20 % polydispersity.	Spherical	Not stated.	[73]
Chemical reduction(micro emulsion)	$AgNO_3$	$NaBH_4$	Natural biosurfactant, rhamnolipid and n-butanol as co-surfactant	6-15 nm	Spherical	Not stated.	[74]
Chemical reduction(micro emulsion)	$AgNO_3$	$NaBH_4$	CTAB	Appr.40 nm	Cube shaped	Antimicrobial activity against *Escherichia coli* and *Candida albicans.*	[46]

Chemical reduction	(PPh_3) Ag-NO_3	Tert-butylamine borane (TBAB)	1-dodecanethiol	2.5 nm	Spherical	Not stated.	[66]
Chemical reduction	(PPh_3) Ag-Cl	TBAB	1-dodecanethiol	4.8 nm	Spherical	Not stated.	[66]
Chemical reduction	(Pph_3) Ag-Br	TBAB	1-dodecanethiol	3.4 nm	Spherical	Not stated.	[66]
Chemical reduction	$AgNO_3$	$N_2H_4{\cdot}H_20$	PVP	50-200 nm	Triangular	Application in surface-enhanced Raman scattering (SERS).	[49]
Chemical reduction(micro emulsion)	$AgNO_3$	$N_2H_4{\cdot}H_20$	Sodium bis (2-ethylhexyl) sulfosuccinate (AOT)	2-5 nm	Spherical	Antibacterial sector.	[75]
Chemical reduction(micro emulsion)	$AgNO_3$	$N_2H_4{\cdot}H_20$	SDS and isoamylalchohol as the co-surfactant	6.5-12.1 nm	Spherical	Not stated.	[47]

Chemical reduction	$AgNO_3$	Aniline	CTAB	10-30 nm	Spherical	Not stated.	[52]
Chemical reduction	$AgNO_3$	Tannic acid	Sodium citrate	Appr.46 nm	Spherical	Not stated.	[58]
Chemical reduction	$AgNO_3$	Glucose	PVP. NaOH enhanced the speed of reaction.	20-80 nm	Spherical	Not stated.	[51]
Chemical reduction (polyol process)	$AgNO_3$	Ethylene glycol	PVP	17 ± 2 nm	Spherical	Not stated.	[50]
Thermal reduction	$AgCF_3COO$	Isoamyl ether	Oleic acid	7-11 nm	Spherical	Not stated.	[76]
Green chemistry (seed extract)	$AgNO_3$	Jack fruit seeds extract		22.12±1.05 nm	Not stated	Antibacterial activities against *Escherichia coli*, *salmonella Enterica Typhimurium*	[77]
Green chemistry (peel extract)	$AgNO_3$	Citrus sinensis peel extract		~35 nm	Spherical	Antibacterial activity against *Escherichia coli, Pseudomonas aeruginosa*	[78]

					and *Staphylococcus aureus*	
Green Chemistry (leaf extract)	$AgNO_3$	*Melia dubia* leaf extract	~7.3 nm	Spherical	Anticancer activity against human breast cancer (KB) cell line.	[68]
Green Chemistry (fruit extract)	$AgNO_3$	Fruit extract *Sterculia acuminata*	~10 nm	Spherical	Catalysis activity	[21]
Green Chemistry (fruit extract)	$AgNO_3$	Fruit extract of *Phyllanthus emblica*	~39 nm	Spherical	Antimicrobial activity *in vitro* against the pathogen *Acidovorax oryzae* strain RS-2 of rice bacterial brown stripe	[79]
Green chemistry (seed extract)	$AgNO_3$	Seed extract of *Alpinia katsumadai*	~12.6 nm	Quasi-spherical	Cytotoxic effect against human gastric carcinoma SGC-7901 and antibacterial activity against Gram-positive	[80]

					bacterium *Streptococcus aureus* and the Gram-negative bacteria *Escherichia coli* and *Pseudomonas aeruginosa.*	
Green Chemistry (leaf extract)	$AgNO_3$	*Moringa oleifera* leaf extract	~50 nm	Spherical and rectangular	Drug Delivery.	[14]

2

3. Nucleation and growth mechanisms and kinetics

Chemical synthesis of AgNPs is a dynamic process, thus, kinetic information, such as rate constants and mechanisms, is required to achieve the desired size and dispersity of particles. A brief description of LaMer model and Ostwald ripening mechanism is provided in this section, and the Finke-Watzky two-step mechanism is identified as the most suitable model to describe the autocatalytic synthesis of different metal-NPs like silver, gold and palladium [81], [82], [83].

The first mechanism used to describe NPs synthesis was developed by LaMer and Dinegar [39], who examined the synthesis of sulphur sols from the decomposition of sodium thiosulfate. According to LaMer model, synthesis starts with a single instantaneous nucleation process. After that, nucleation ceases to occur as a consequence of low monomer concentration. Following nucleation, growth takes place by the diffusion and incorporation of the monomers in the solution. More specifically, this model suggests that a spherical volume with radius h has a concentric spherical nucleus with radius x where growth takes place on the surface of the spherical nucleus upon the arrival of a diffusing monomer. **Eq. (1)** shows the mathematical expression for the temporal evolution the radius x:

$$\frac{d}{dt}(x^2) = [C_{ss} - C_s(t)]\frac{2D}{\rho} - \frac{2D}{h^3}x^3, \quad \textbf{(1)}$$

where C_{ss} is the supersaturation concentration of sulfur, $C_s(t)$ is the concentration of the soluble "monomer" above the saturation concentration as a function of time, D is the diffusion coefficient, p is the bulk density of elemental sulfur.

The Ostwald ripening mechanism was expressed by Lifshitz and Slyozov [40] and Wagner [84] (LSW theory). The mathematical theory of this growth mechanism is based on the high solubility and the surface energy of smaller particles in a solution, which redissolve, thus allowing the larger particles to grow further. Piwoński, Spilarewicz-Stanek [85] and Shukla, Joshi [86] discussed Ostwald ripening mechanism in the growth of silver and silver halide particles, respectively. In this model, the radius r of the particle varies with time, as described in **Eq. (2)**:

$$\frac{dr}{dt} = \frac{D}{r}\left(\Delta - \frac{a}{r}\right), \quad \textbf{(2)}$$

where $\Delta = c - c_\infty$, is the difference of current concentration (c) and saturated concentration (c_∞) of a solution, D is the diffusion constant, and $a = {}^{2\sigma u c_\infty}/_{RT}$ is defined by the surface tension σ, solubility c_∞, atomic volume u of the solute, gas constant R , and temperature T.

The Finke-Watzky two-step mechanism [38] assumes a slow continuous nucleation followed by an autocatalytic growth step. The concentration of precursor A remains almost constant for a long time and then a quick sigmoidal decrease is observed. During the first step, there is a direct formation of nuclei from precursor A through a pseudo-first order reaction, illustrated in **Eq. (3)**:

$$Nucleation: A \xrightarrow{k_1} \mathrm{B} \quad ; \quad n_0 = k_1[A], \quad \textbf{(3)}$$

where k_1, n_0, and $[A]$ correspond to the nucleation kinetic constant, the nucleation rate, and the molar concentration of the precursor, respectively. After nucleation, an autocatalytic growth of B nuclei and the formation of B particles follows, as shown in **Eq. (4)**:

$$Growth: A + B \xrightarrow{k_2} 2B \quad ; \quad G = k_2[A][B], \quad \textbf{(4)}$$

where k_2, G, and $[B]$ correspond to the growth kinetic constant, the growth rate, and the molar concentration of the silver nuclei, respectively. Assuming that the concentration of nuclei [B] changes with time *t* as $[B](t) = [A]_0 - [A](t)$, where [A](t) is the concentration of precursor at time t and $[A]_0$ is the initial concentration of the precursor, [A] depends on time as shown in **Eq. (5)**:

$$[A](t) = \frac{\frac{k_1}{k_2} + [A]_0}{1 + \frac{k_1}{k_2[A]_0} * exp(k_1 + k_2[A]_0)\, t}. \quad \textbf{(5)}$$

Values of rate constants k_1 and k_2 can be obtained from fitting **Eq. (5)** or from its linearized form (**Eq. (6)**):

$$ln\left(\frac{[A]_0 - [A]}{[A]}\right) = ln\left(\frac{k_1}{k_2[A_0]}\right) + k_2[A]_0 t, \quad \textbf{(6)}$$

obtained under assumptions $k_1 \ll k_2[A]_0 \; and \; [A] < [A]_0$ [87].

The autocatalytic behaviour of transition metals like silver and gold cannot be described through LaMer model. This model requires super saturation conditions to initiate burst nucleation while the autocatalytic mechanism takes place for reactions far below supersaturation conditions as a result of a slow kinetic conversion of the metal precursor to an active monomer [88].

The Finke-Watzky mechanism has been used in several publications for a complete description of the kinetics of synthesis of AgNPs with different methods being used for the determination of the rate constants for nucleation (k_1) and growth (k_2). Some relevant examples are described below and summarized in **Table 2**. Kytsya, Bazylyak [89] studied and estimated the kinetics of the synthesis of AgNPs using the method of direct potentiometry. AgNPs were obtained by the reduction of silver nitrate with hydrazine at basic pH and sodium citrate as stabilising agent. The authors verified the use of the Finke-Watzky two-step mechanism in AgNP formation and reported that the nucleation of AgNPs is limited by the reduction of silver ions to silver atoms. For this reason, they proposed a surface-dependent model for AgNP growth based on Finke-Watzky model, which leads to equations that describe the total reaction rate. A similar study is described by Sandoe, Watzky [90], who measured the change in AgNP surface plasmon resonance and change in silver ion concentration during citrate method for the synthesis of AgNPs using UV-visible spectroscopy (indirect method) and ion-selective electrode potentiometry and atomic absorption spectroscopy (AAS) (direct method). The sigmoidal kinetic curves obtained were described by Finke-Watzky model and the rate constants for nucleation (k_1) and growth (k_2) were estimated for each method separately. Sandoe, Watzky [90] showed that the average values of k_1 and k_2 overlapped within experimental error between the different methods. Amirjani and Haghshenas [87] also indicated that the nucleation and growth of AgNPs is very similar to the Finke-Watzky mechanism. The authors used three different approaches to model the kinetics of the synthesis process including linear fitting, non-linear fitting and a modified Finke-Watzky mechanism by considering a reversible pseudo-first order reaction for the nucleation step. Their kinetic data were obtained by borohydride reduction with PVP and showed significant differences between the

three different approaches. In the case of 0.0008 g PVP and linear Finke-Watzky mechanism, k_1 and k_2 were estimated to be 0.034 ± 0.0001 min^{-1} and 911 ± 6 $M^{-1}min^{-1}$, respectively. For the same conditions but non-linear fitting, k_1 and k_2 were calculated to be 0.031 ± 0.01 min^{-1} and 574 ± 5 $M^{-1}min^{-1}$, respectively. By using a modified Finke-Watzky mechanism, the authors developed a kinetic model closer to the synthesis system with k_1 and k_2 equal to 1.025 ± 0.003 min^{-1} and 107.7 ± 5 $M^{-1}min^{-1}$, respectively. By estimating k_1 and k_2 at different concentrations of PVP, they also showed that PVP can hinder both the nucleation and growth stages.

The improvement and development of kinetic models for AgNPs synthesis is still an open field of research. Specifically, there is a need to develop a kinetic model suitable for using in numerical simulations which simultaneously account for the process of hydrodynamics, as will be described in detail in the upcoming sections.

Table 2: Examples of nucleation (k_1) and growth (k_2) constants of Finke-Watzky model for synthesis of AgNPs using different methods and reagents. All the rate constants k_1 and k_2 were converted into min^{-1} and $M^{-1}min^{-1}$, respectively from the original publications.

Method/Reagents	k_1 (min^{-1})	k_2 ($M^{-1}min^{-1}$)	References
Chemical reduction/Silver nitrate, sodium hydroxide, hydrazine hydrate, sodium citrate dihydrate at 20°C.	9×10^{-6} min^{-1}	959 M^{-1} min^{-1}	[89]
Chemical reduction/Silver nitrate(0.2mM), sodium citrate (1 mM), (UV-visible spectroscopy).	$(2.2\pm0.4) \times 10^{-5}$ min^{-1}	(0.53 ± 0.01) $M^{-1}min^{-1}$	[90]
Microwave technique/ Silver nitrate, ethylene	$(1.3\pm0.6) \times 10^{-8}$ min^{-1} at 180°C	$(24.1\pm0.6) \times 10^{-2}$ $M^{-1}min^{-1}$ at 180 °C	[81]

glycol, PVP at 130-180^{0}C	(2±0.2) × 10^{-5} min^{-1}at 130^{o}C	(1.65±0.02) × 10^{-2} $M^{-1}min^{-1}$ at 130^{o}C	
Chemical reduction/Silver nitrate(2.5mM), trisodium citrate dihydrate (0.1 M), sodium borohydride (1.25mM, PVP (7.2 x 10^{-6} mole) (non-linear fitting).	0.031 ± 0.01 min^{-1}	574 ± 5 $M^{-1}min^{-1}$	[87]
Photoreduction of silver perchlorate in water/AOT/benzene water in oil(w/o) microemulsions.	9 × 10^{-3} min^{-1}	71 × 10^{-2} $M^{-1}min^{-1}$	[91]
Reduction of silver nitrate (0.012M) by hydrazine (0.66 M) in the reverse micelles of oxyethylated surfactant Triton N-42 at 25^{o}C.	9.59 × 10^{-3} min^{-1}	1.848 × 10^4 $M^{-1}min^{-1}$	[92]

4.Parameters affecting the physicochemical properties of AgNPs

Since tightly-defined properties of AgNPs are necessary for many industrial applications, the control and determination of the reaction conditions to achieve a reproducible synthesis process and to avoid polydispersity are critical. Some experimental parameters can be tuned to control AgNPs size, shape,

and stability, including reagents concentration, reaction temperature, pH of the solution, use of a complexing agent, and mixing rate, among others.

Firstly, the size and shape of AgNPs can be controlled by adjusting the type and concentration of the reducing agent and silver precursor [93], [34]. Sobczak-Kupiec, Malina [94] found that the increase in the concentration of the precursor used (silver nitrate) leads to larger particles because of an increased collision frequency. By preparing AgNPs using different silver phosphine precursors, such as RAg (PPH_3)n (R=Cl, Br, or NO_3 and n=1 or 3), with tert-butylamine borane (TBAB) in the presence of dodecanethiols (C_{12}), Andrieux-Ledier, Tremblay [66] showed that the nature of the functional group in the silver precursor affects the AgNPs size as well. The authors assumed that the small raise of the redox potential (NO_3Ag (PPH_3) > BrAg (PPH_3) > ClAg (PPH_3)) results in a significant rise of the nucleation rate and hence a reduction in the size of AgNPs from Cl to Br and Cl to NO_3, respectively.

Regarding the type of reducing agent, Demchenko, Riabov [95] showed that decreasing redox potentials of reducing agents results in larger NPs. Specifically, use of sodium borohydride ($NaBH_4$) as a strong reducing agent can facilitate instant nuclei generation, leading to the formation of smaller NPs, while a weaker reducing agent, such as ascorbic acid, produces bigger NPs. When using weak reductants, the reaction rate can be raised by raising the temperature [67]. Skrabalak, Wiley [96] presented a study on how the polyol synthesis can be used to produce AgNPs with different shapes, such as nanowires and nanocubes. They showed that heating ethylene glycol in air results in its oxidation to glycolaldehyde (GA), a powerful reducing agent. The temperature of reaction strongly affects the amount of GA produced and hence the reduction rate. For the interested reader, Mukherji, Bharti [97] reviewed different approaches that can be used for the synthesis of AgNPs of a desired size and shape.

As another example of the temperature effect, Kaviya, Santhanalakshmi [78] prepared spherical AgNPs at room temperature (25 ℃) and 60℃ using citrus sinensis peel extract as the reducing and capping agent. The sizes of AgNPs were 35 nm and 10 nm at 25℃ and 60 ℃, respectively. Similarly, Liu, Zhang [98] examined the effect of temperature on the nucleation and growth kinetic constants. They showed that the nucleation rate constant increases sharply at high temperatures, while the growth rate constant

rises linearly with the reaction temperature. The authors concluded that the decrease of particle size at high temperatures can be attributed to the sharp rise in the nucleation constant instead of the reduced growth rate constant. For microfluidic synthesis, temperature control is possible using glass based microreactors such as borosilicate [99].

As mentioned previously, the morphology and size of AgNPs can be controlled by the addition of complexing agents. Some common complexing agents include ammonia (NH_3) [100] and ethylenediaminetetraacetic acid (EDTA) [101]. V. Goia and Matijević [59] demonstrated the changes in redox potentials of Ag^+ as a consequence of complex formation. For example, NH_3 and Ag^+ form Ag $(NH_3)_2^+$, which shows more difficulty to be reduced to Ag^o compared to Ag^+ as the stability of its complex increases. The redox potentials of [Ag $(NH_3)_2$] $^+/Ag^o$ and Ag^+/Ag^o are 0.38 V and 0.799 V, respectively. Therefore, when the reaction takes places in the presence of Ag $(NH_3)_2$, ethylene glycol and PVP, the growth of silver grains is supressed leading to smaller size of AgNPs, as investigated by Zhao, Sun [100]. An interesting example in the literature is also described by Feng, Ruan [101]. They reported that Ag/EDTA complex significantly reduces the reaction speed of AgNPs and thus makes its crystalline growth have good selectivity.

Another factor that affects particle size and shape is pH. Alqadi, Abo Noqtah [102] studied the effect of pH on the aggregation of AgNPs synthesized by chemical reduction and showed that the size decreases with an increase in pH. Marciniak, Nowak [103] studied the effect of pH on the size of AgNPs using citric acid. At alkaline conditions, they observed that the charges of citrate (pka =6.4) change and dicarboxyacetone (DCA) is produced as a by-product of the decarboxylation of citrate during silver reduction. At a pH value of 12, there is a completely hydrolysed DCA^{2-} and Cit^{3-} species, and a higher reducing ability leading to faster reduction of the silver ions during the growth stage. Similarly, Qin, Ji [104] presented that high pH improves the reducing power of ascorbic acid and smaller size particles can be obtained. Similarly, Qin, Ji [104] presented that high pH improves the reducing power of ascorbic acid and smaller size particles can be obtained. The influence of pH on the shape of AgNPs has been discussed in detail by Dong, Ji [105]. The authors used citrate reduction of silver nitrate under high and low pH (from 5.7 to 11.1) and developed a stepwise reduction method to

have a better control over the shape of AgNPs. At high pH, AgNPs were both spherical- and rod-like due to fast reduction rates of silver nitrate, while at low pH AgNPs were triangle- and polygon-shaped as a result of slow reduction rate of silver precursor. They proposed a fast nucleation stage at high pH followed by a slow growth stage in lower pH to improve the balance between the nucleation and growth processes.

The effect of mixing on AgNPs size has also been investigated. Ng, Chen [106] synthesized AgNPs through a green chemistry method using a rotating packed bed reactor. The intense mixing and high mass transfer rates led to more uniform and smaller-sized AgNPs. Similarly, Kisyelova, Novruzova [107] used a stirred tank reactor (STR) with a turbine impeller and a spinning disc reactor (SDR). They showed that these reactor configurations can intensify the mixing process and reduce the average size of AgNPs from 31 to 16 nm.

Generally, AgNPs tend to agglomerate and gradually grow into larger particles to reduce their overall surface energy. Therefore, to preserve the targeted mean size and particle size distribution of synthesized AgNPs, it is important to use a stabilising agent. Multiple mechanisms of AgNPs stabilisation by capping agents are found in the literature, including steric, electrostatic, or electro steric stabilisation. Ionic stabilisers (e.g., citrate) generate a charged layer around particles that serves as an electrostatic barrier to agglomeration. More specifically, repulsive forces are created between NPs and, provided the electric potential related to the double layer is high enough, the electrostatic repulsion will inhibit aggregation [108]. According to Badawy, Luxton [109], uncoated AgNPs have Z-potential -22 mV, while AgNPs stabilised electrostatically through the ionization of the carboxyl groups of citrate have -40mV. The electrostatic stabilisation can be influenced by pH, temperature, and concentration of stabilising agent.

On the other hand, non-ionic compounds can be adsorbed onto the surface of the NPs and provide a steric protective layer. The thickness of this protective layer depends on the nature of the stabilising agent. The incorporation process of non-ionic molecules depends on surface properties of NP. For example, noble metals such as silver are well bonded with thiols, amines, and cyanides [110]. The adsorbed molecules are limited in free motion leading to a reduction of entropy and in this way to an

increase of free energy [108], [111]. Examples of non-ionic stabilisers are PVP and PEG. It has been reported that AgNPs sterically stabilised by PVP and PEG are more stable than citrate-coated AgNPs, which weakly interact with the Ag core and stabilise AgNPs through charge repulsion [112]. However, the main advantage of citrate in AgNPs synthesis is the opportunity of further functionalisation of NPs as citrate can be easily replaced by other compounds. This is a consequence of the weak interactions of citrate molecules with metal surfaces.

An interesting study that combined the two mentioned protective mechanisms was conducted by Wang, Li [113]. They used the steric hindrance effect of PVP and the charge repulsion effect of sodium tripolyphosphate (STPP) to observe differences in dispersity, stability, and redox process of AgNPs synthesis. The synergistic effect of both PVP and STPP limited the reaction rate of silver ions preventing by this way the polydispersity of NPs.

It is worth mentioning that the size of AgNPs is based on the electron-donating capacity of the capping agent. For example, AgNPs of sizes from small to large can be obtained in the following order: PVP<citrate<SDS. This occurs because PVP has a higher electron-donating tendency, resulting in stronger interactions with positively-charged silver ions during the reduction step and thus an improved stabilisation [114].

Aside from the parameters directly involved in AgNPs synthesis, storage conditions, storage time, and the stabilisation mechanism can also affect the temporal evolution of the AgNPs properties. According to Izak-Nau, Huk [115], AgNPs dispersion can age during storage and the most significant factors affecting ageing are temperature, exposure to daylight, and the nature of the stabilising agent. The changes that can been seen during ageing are related to processes of agglomeration, dissolution, or oxidation. In the case of dispersions stored at room temperature and exposed to daylight, an increase in particle size was observed. An increase of temperature results in an increase of NP collision rate, which causes agglomeration, while the exposure to daylight induces the photo-reduction of already dissolved Ag ions and the generation of new AgNPs increasing the sample's dispersity. Regarding the nature of the stabilising agent, it was found that AgNPs coated by neutral stabilisers demonstrate better stability over time compared to the AgNPs stabilised by positive and negative stabilisers. Particularly, Izak-Nau,

Huk [115] showed that negative and positive capping agents may cause agglomeration at room temperature. Other observed effects during ageing are related to dissolution and oxidation of AgNPs, which may change the composition of samples and modulate their toxicity. For example, in the case of negatively charged AgNPs samples, it was shown that longer storage time leads to an increase in the amount of Ag ions. An explanation for this behaviour could be related to the stabilisation mechanism as neutral AgNPs were stabilised sterically, while positively and negatively charged AgNPs were stabilised electrostatically [115].

5. Synthesis and properties of silver nanoparticles: computational and numerical studies

This section contains a summary of the most relevant computational and modelling studies made in the field of AgNPs synthesis, their properties, and their interactions with a third component, such as capping agents. The literature regarding the modelling of AgNPs can be divided into two main categories according to the general approach followed. The first is based on data-driven models, namely, models built upon data-set inputs obtained from either experimental measurements and/or computational simulations. The second corresponds to physics-based models, which span across a broad range of time and length scales depending on the degree of accuracy and the main phenomena aimed to capture. These models usually require a set of conservation equations that describe the motion of individual entities or fluids and a set of initial and boundary conditions of the system.

Figure 2 depicts a summary of the aforementioned categories. The physics-based models can be divided, in turn, into two additional sub-sections according to the scale of interest. The numerical studies specifically related to microfluidic channels are included in **Figure 2** and are discussed in §5.3 and in more detail in §6 along with the main experimental discoveries. For the interested reader, Pedregosa, Varoquaux [116], Allen and Tildesley [117], Andersson, Andersson [118], and Marchisio, Fox [119] provide a comprehensive theoretical and practical description of data-driven models, MD, CFD and PBM, respectively, including mathematical and physical concepts related to each method, the necessary input and output parameters for simulations, and their use in a wide range of engineering applications.

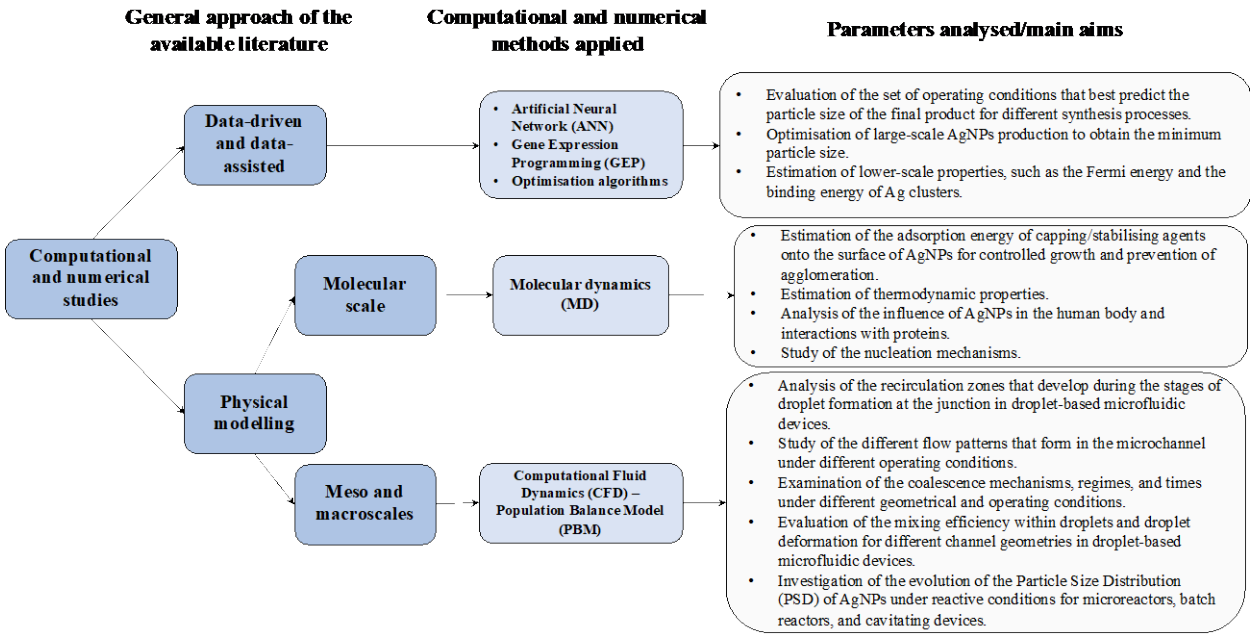

Figure 2: Summary of the computational and numerical literature related to AgNPs, the categories used for classification of the available studies, and the main parameters analysed. It is relevant to note that, while the approaches of physics-based models are divided depending on the scale of interest, data-driven approaches are used to estimate parameters from the molecular scale to the macroscale.

5.1. Data-driven and data-assisted models

In recent years, data-driven methodologies, especially those related to Artificial Intelligence (AI) and Machine Learning (ML), have become a nexus for many engineering and scientific disciplines, including the production of nanotechnology [120]. This section is not intended to be a comprehensive account of all the existing models and their numerous applications in the field of nanomaterials. Rather, it provides a general examination of how these data-based methodologies have been and can be used to extract relevant information about AgNPs. For the interested reader, Furxhi, Murphy [121] give an in-depth review of the many ML techniques that have been applied to the topic of nanomaterials.

In the specific field of AgNPs synthesis, data-driven models have been employed almost exclusively to understand and predict the complex relationships between multiple operating conditions, such as temperature and concentration of the reactants, and the properties of the final product. The motivation for analysing such relationships arises from the current need for tightly-controlled and optimised

processes that lead to AgNPs with monodisperse properties, especially in terms of size. The available literature has mainly leveraged the characteristics of multi-layer Artificial Neural Networks (ANN) over other data-based models given their suitability to establish condition-property relations [120].

Relevant works in the area of ANN used to predict particle size are represented in Shabanzadeh, Senu [122] and shafaei and Khayati [123]. The former investigates a synthesis route where silver nitrate is reduced using sodium borohydride in the presence of a clay (montmorillonite, MMT) compound that supports the NPs within its interlamellar spaces to avoid agglomeration. The input parameters for the network were the concentration of silver nitrate, the reaction temperature, the UV-visible wavelength, and the spacing of the MMT interlayer. It was found that the concentration of silver nitrate and the temperature were the most influential parameters for the prediction of the particle size. The study shafaei and Khayati [123] was devoted to predicting and minimising the particle size of AgNPs obtained from a green synthesis process that used silver nitrate and opium syrup as reactants in a semi-batch process. The operating conditions considered in the model were the precursor to reducing agent ratio, the volumetric feed rate, the pH, the temperature, and the agitation speed. The authors found that the particle size is more influenced by the feed rate, the precursor to reducing agent ratio, and the stirring rate than by the other parameters.

Evolutionary algorithms have also been found useful to predict particle size. In Sattari and Khayati [124], Gene Expression Programming (GEP) was employed to predict the particle size of AgNPs prepared by a green synthesis method in which silver nitrate acted as the precursor and a plant extract acted as the reducing agent. Similar to Shabanzadeh, Senu [122], Sattari and Khayati [124] suggested that the initial concentration of silver nitrate was one of the best estimators of the final particle size.

Recently, the literature has moved to expand the application of data-driven methodologies not only to predict the particle size for a given set of conditions, but to include additional properties and to assist the fabrication of samples with targeted properties. Mekki-Berrada, Ren [125] have proposed a two-step ML framework to produce AgNPs with the desired absorbance spectrum. This framework combines the advantages of a high-throughput droplet-based microfluidic experimental setup with Bayesian Optimisation (BO) and Deep Neural Network (DNN) to establish non-trivial connections

between the chemical composition of the inlet reactants and the absorbance spectrum of the NPs. For example, the framework was able to predict that the ratio between the inlet flow rate of the capping agent and the silver precursor has the highest influence on the shape of the absorbance spectrum. As for properties at lower scales, Sun, Fernandez [126] analysed the relationship between various structural, morphological, and geometrical features of AgNPs and their Fermi energy. The authors of this study employed a series of ML-related algorithms, such as ANN regression, logistic regression (LR), random forest modelling (RF), principal components analysis (PCA), and k-fold cross validation to characterise and predict the aforementioned relationship.

The available literature demonstrates that data-driven models offer promising tools to unravel the intricate relationships between various operating parameters with industry-relevant properties, such as size, as well as to successfully manufacture NPs with specific properties of interest. Nonetheless, it is apparent that the application of data-driven models to the synthesis of AgNPs is still an emerging topic whose potential is yet to be explored to the fullest. Despite a few limited examples, the predicting capabilities of data-driven methods for properties different than size have not been tested yet. The numerous special properties of AgNPs, which make them suitable to diverse applications, justify the prevailing need to apply ML-based methods to estimate additional properties. As high throughput experimental methods, such as microfluidic devices (mentioned in detail in §6), and physics-based simulations (mentioned in §5.2-§6) become more relevant for AgNPs synthesis, expanded datasets will become readily available. Thus, there is an opportunity for the generation of integrated frameworks between experiments, simulations, and data-driven models for experimental planning, property prediction, and capturing of the underlying physics of the system.

5.2. Physics-based models: Molecular dynamics simulations of AgNPs

Molecular-scale investigations of AgNPs have been conducted via MD simulations primarily to study the interactions between the forming NPs and a third agent, which may be a protein in the human body for drug-intake applications, as seen in Hashemnia, Zarei [127] and Hazarika and Jha [128], or a stabilising/capping agent. MD simulations are especially important for this topic since these interactions

have a strong influence on the growth mechanisms of the NPs, which, in turn, affect the final particle size and shape, as mentioned previously in §4. Additionally, the molecular interactions among these components can be directly accounted for at this simulation scale without significant simplifications or closing assumptions. MD have also been found useful for estimating thermodynamic properties, as seen in Luo, Hu [129], and understanding the nucleation and growth mechanisms, as seen in Yoneya and Sugisawa [130].

Multiple MD studies can be identified in the literature regarding PVP capping agents specifically and their role in the formation process of AgNPs. This particular structure-directing agent has been of interest given the flexibility and versatility it provides in the synthesis and control of NPs of different shapes, including cubes, nanosheets, nanoplates, and nanowires [131]. It has been shown experimentally that the regio-selective adsorption of PVP to the surface of the NPs causes different growth kinetics in different planes, which is a concept used to produce particles of various shapes [132]. The interaction energy between PVP and different crystal planes of AgNPs has been estimated by MD in Mdluli, Sosibo [133] for isolated NPs and Qi, Balankura [134] for NPs in the presence of ethylene glycol, which acts as a reducing agent in most PVP-mediated AgNPs synthesis processes. These studies demonstrated that PVP has a preferred plane of adsorption, determined by the highest attraction interaction energy between the PVP molecule and the NP. By calculating the atomic density profile in the NP's surface, these studies were also able to confirm that the oxygen atom of the carbonyl group in the pyrrolidone ring of PVP tends to be closer in proximity to the Ag surface than the other atoms, which elucidates a kinetically-favoured interaction between this atom and the NP (see **Figure 3** A).

Similarly, Kyrychenko, Korsun [135] investigated the adsorption, wrapping, and coating of PVP oligomers of different lengths around a small (4.5 nm) silver core in aqueous solutions through MD simulations. The main objective of this work was to identify the oligomer length that would result in the most effective protection of the core against interactions with water and aggregation with other NPs, which would increase the polydispersity of the sample. It was found that a single, long-chain PVP oligomer results in better core shielding than a mixture of multiple short-chain oligomers (see **Figure 3** D). Meneghetti, Soares [131] used MD simulations to gain a better understanding of the adsorption

mechanism of PVP to the surface of a silver NP in the presence of both pure ethylene glycol solution, and the same solvent with $AgNO_3$ or NO, which represent more realistic scenarios for AgNPs synthesis. The authors showed that the PVP molecule forms an ordered and compact layer on the surface of the Ag plane in presence of pure ethylene glycol in solution or with $AgNO_3$ (Ag^+ and NO_3^- ions in solution). In contrast, when NO is present, the PVP polymer tends to expand on the Ag surface.

Balankura, Yan [136] and Balbuena, Gianetti [137] also provided information related to the synthesis and aggregation of Ag nanostructures in the presence of PVP through MD simulations. In the case of Balankura, Yan [136], the aggregation mechanism of PVP-coated triangular Ag nanoplates in a vacuum and in the presence of ethylene glycol was analysed. Their results suggest that the attachment occurs when the PVP molecules either diffuse or desorb to leave a vacant space for aggregation and that the free energy barrier needed for attachment is significantly higher for face-to-face aggregation than for lateral aggregation. This lower energy barrier was ascribed to the lower concentration of PVP found in the lateral faces of the surface of the NPs. Balbuena, Gianetti [137] investigated the nucleation and growth dynamic mechanisms of AgNPs in the presence of PVP and ethylene glycol. A detailed analysis of the complex steps that lead to NP formation was provided, and it was found that PVP does not have a significant influence on NP growth during the first $\sim 0.1\, ns$. Nevertheless, for longer simulation times, the PVP tends to act either as a "bridge" between particles, promoting growth, or as a "shield", hindering it.

As for other types of capping agents, Zeng, Jiang [138] investigated the growth mechanisms of AgNPs in the presence of different surfactants to obtain better control of the particle shape, which is desired for various applications. The growth mechanisms were studied through the estimation of the interaction energies between the surfactants and different Ag crystalline planes (100, 110, 111). The tested surfactants were bis(2-ethylhexyl) sulfosuccinate (AOT), 1-dodecanethiol ($C_{12}SH$), and cetyltrimethylammonium bromide (CTAB). It was shown that all the surfactants have the same preferred plane of adsorption (111, lowest interaction energy), which would impede crystal growth in that direction and influence the final shape of the NPs.

In a similar work, Yang, Chen [139] used MD to study the interactions between positively-charged AgNPs and cetyltrimethylammonium cations capping agents (CTA^+) at the molecular scale. These simulations were able to demonstrate that the head's functional group is the part of the CTA^+ molecule that adsorbs onto the Ag core and contributes to the overall stability of the NP. The work of Kyrychenko, Pasko [140] aimed to understand the role of single-chain poly(vinyl alcohol) (PVA) capping agents of different lengths in preventing the interaction between AgNPs and water. The authors provided evidence to suggest that multiple non-covalent interactions occur in the adsorption process of PVA onto the surface of Ag, and that the interactions of the hydroxyl groups of the PVA polymer have a significant influence on the whole process (see **Figure 3** B). This study also pointed out that the length of the polymer chain has a direct effect on the coverage of the NP's surface and that, for the longest chain tested (1540 monomers), the PVA was able to protect about 90% of the Ag surface from contact with water (see **Figure 3** D).

Recent examples of MD investigations regarding the nucleation process of AgNPs are Milek and Zahn [141] and Yoneya and Sugisawa [130]. Milek and Zahn [141] simulated the formation of AgNPs from silver nitrate in the presence of ethylene glycol in solution. More specifically, this study analysed the association of Ag^+ ions and the dynamic evolution of the structure of Ag clusters under different conditions of redox potential. The simulation results were able to confirm that the redox potential plays a key role on the overall shape of the cluster and its internal structure. Yoneya and Sugisawa [130] simulated the formation of AgNPs in a thermal synthesis process where silver oxalate acts as the precursor and oleyl amine as the stabiliser. The results of Yoneya and Sugisawa [130] suggested that the growth of the NPs was driven by the aggregation/coalescence of Ag clusters after the thermal reduction of the precursor and the liberation of CO_2 molecules.

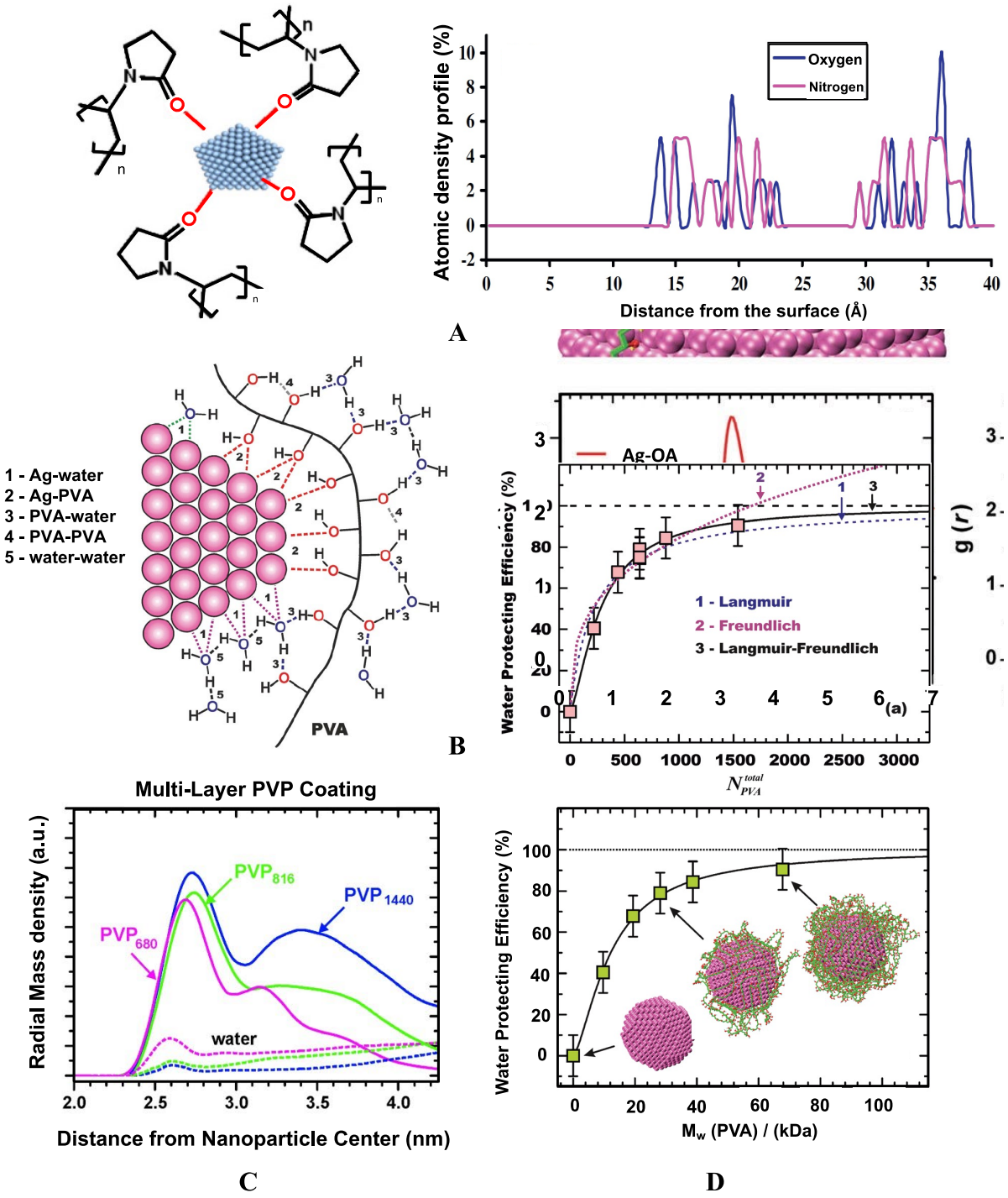

Figure 3: Bonding configurations of PVP (A) and PVA (B) capping agents, multi-layer PVP coating around the AgNP core (C), and efficiency of water protection by PVA adsorption (D). A) Oxygen from the carbonyl group of the PVP molecule is located closest to the NP surface, as shown by the schematic diagram (left) and the atomic density profile (right). Images from [133]. B) Oxygen atom from the hydroxyl group of the PVA molecule is the most frequently found bond in the presence of water, as shown in the schematic representation (left) and the radial distribution function (right). Images from [140]. C) Influence of the number of repeating PVP units on the radial mass density function, depicting a multi-layer coating

configuration. Image from the simulations of [135]. D) Water protecting efficiency of PVA as a function of the molecular weight of the capping agent molecule. Image from [140].

As elucidated from the studies discussed in this sub-section, MD simulations have several key characteristics that allow them to provide helpful information about AgNPs in terms of understanding how different particle sizes and shapes can be obtained using different stabilising agents. This piece of information can be crucial during the designing stages of new stabilising agents and new synthesis routes when selecting the appropriate reactants to obtain specific properties. Important characteristics of MD relate to the ability to consider different type of interactions between different atoms and tracking molecular trajectories of multiple entities. MD-related techniques are nonetheless markedly limited by the short time and lengths scales (usually in the order of nano) that can be simulated with present-day computational tools. In order to investigate broader systems and include other phenomena, such as hydrodynamics, models at the meso- and macro scales are needed.

5.3. Physics-based models: Meso/macroscale studies that involve chemical reactions for different synthesis methods (PBM-CFD simulations)

This sub-section is dedicated to the computational/numerical studies on the meso- and macroscales that specifically include chemical reactions of AgNPs synthesis in different reactors. Compared to aspects pertaining the hydrodynamics of the system in microfluidic devices, such as droplet formation and mixing, which will be addressed in the following section, the area is considerably less investigated, indicating the need for more extensive studies. In general terms, a description of the system at the meso- and macroscales through numerical simulations is the basis for build-up of surrogate models able illustrate the evolution of the size and size distribution of the NPs and how these properties are affected by relevant operating conditions. Among these conditions, the type, geometry, and operating regime of the reactor, the flow rates of the reactants, and the mixing rates are the ones that have sparked the most interest in the literature. Two of the most common computational techniques at the meso- and macroscales are PBM and CFD, respectively, given their suitability to be coupled with each other and

their ability to describe a large population of polydisperse entities at a lower computational cost than other approaches, such as a purely Lagrangian framework.

The first study that attempted to simulate the synthesis reactions of AgNPs in the meso- and macroscales was by Liu, Li [142]. They employed a PBM and CFD framework with reactive kinetics to predict the Particle Size Distribution (PSD) of AgNPs synthesised in a straight, continuous-flow microchannel. The basis of the PBM framework is the mesoscale description of a population of discrete sub-entities (i.e., nanoparticles) and their PSD evolution is described by means of a population balance equation (PBE). A PBE refers to a kinetic transport equation in terms of the number density function (NDF), which quantifies the number of particles with a particular property or internal variable per unit volume. For the case in which particle size L is an internal variable, the NDF $f(L, \mathbf{x}, t)$ is defined in such a way that $f(L, \mathbf{x}, t)dLd\mathbf{x}$ corresponds to the number of particles with size L expected to be found at position $\mathbf{x}$ in physical space. The general form of the PBE adopted by Liu, Li [142] is shown in **Eq. (7)**:

$$\frac{\partial}{\partial t} f(L, \mathbf{x}, t) + \nabla \cdot \left(\mathbf{u_p} f(L, \mathbf{x}, t) \right) = -\frac{\partial}{\partial L} \left(G(L) f(L, \mathbf{x}, t) \right), \qquad (7)$$

where $\mathbf{u_p}$ is the velocity of the particles, and $G(L) \equiv \frac{dL}{dt}$ represents the phenomenon of continuous size-dependent particle growth. The version of the PBE proposed by Liu, Li [142] is the result of assuming that the population of AgNPs only exhibits polydispersity in terms of particle size. Hence, other characteristics, such as the particle velocity ($\mathbf{u_p}$), have a uniform distribution, making the NDF univariate. In addition, the transport of the NDF by means of molecular diffusion was neglected, together with terms that account for discrete events, such as agglomeration and de-agglomeration of the particles. Nucleation of AgNPs was not included explicitly in the NDF equation, but was considered through a boundary condition $f(L = 0, \mathbf{x}, t)G(L) = n_0$, where n_0 represents the nucleation rate [142].

The nucleation and growth rates were based on the Finke-Watzky two-step mechanism discussed in §3 in which a slow nucleation process is followed by an autocatalytic growth (see **Eq. (3)-(4)**). The kinetic

constants k_1 and k_2 ($k_1 << k_2[A]_0$) were estimated from a model-assisted experimental approach developed by the same authors in a previous study [143].

Liu, Li [142] adopted a two-phase mixture model with one continuous liquid phase and one dispersed solid phase. The continuous phase had two chemical species, silver nitrate as the silver precursor, and *Cacumen platycladi* as the reducing and capping agent. The moment transformation was applied to the transport equation for the NDF, and the PBE was solved through the quadrature method of moments (QMOM) [119, 144]. The mean particle size and PSD were analysed under different conditions of flow rate, reactor material, and reactor diameter. In the simulations, the effect of the change in the reactor material, which translated into a change in the interfacial effect between the walls and the fluids in the channel, was accounted for by modifying the kinetic parameters of nucleation and growth. It was found that the average particle size decreased with an increase in the flow rate of the continuous phase and that a decrease in the reactor diameter promotes nucleation and growth by enhancing the interfacial effect, increasing the average size of the particles.

The work of Madadelahi and Shamloo [145] is possibly the first to simulate the mixing process inside droplets and the synthesis reactions in droplet-based microreactors simultaneously. The system considered in this study is a planar serpentine microreactor with a T-junction. Given the nature of droplet-based synthesis of NPs, the authors considered a full CFD approach without PBM. The multiphase flow was treated with the Volume of Fluid (VOF) approach and a continuum surface-force (CSF) model. Besides the continuity and momentum equations, each component of the system in the aqueous phase had a mass-conservation equation to account for mass transfer due to the chemical reaction occurring. Different values for the reaction rate were considered. The mixing inside droplets was quantified in a similar manner as in the studies mentioned in §6.2. The influence of the water fraction (WF, i.e., ratio of the flow rate of the dispersed phase over the total flow rate) on several characteristics of the mixing process and the reaction was investigated. It was found that, with or without reaction, higher WF values result in lower mixing qualities at the same distance covered by the droplet. In accordance with previous studies, when the droplet had not reached the turns and bends of the channel, the mixing efficiency remained lower than 10%. Nonetheless, as soon as the droplets

occupied the first bend of the channel, the mixing quality sharply increased. The improved mixing efficiency at the turns and bends of the channel was attributed to the inertial effects promoted in the bends that create Dean vortices, which promote dissipation of any concentration gradients much more rapidly than streamwise laminar flow in straight channels.

The fabrication of AgNPs in other types of reactors has also been investigated via simulations at the meso- and macroscales. Liu, Lu [146] studied the green synthesis of AgNPs in a hydrodynamic contracting cavitation device via CFD-PBM simulations. Unlike synthesis in microfluidics, the presence of vapour leads to a three-phase turbulent liquid-solid-vapour flow, adding additional levels of complexity to the simulations. The mixture model with no slip velocity was used to treat the three-phase flow, including suitable transport equations for each chemical species with source terms to account for the production/consumption due to chemical reactions. The PSD and average particle size obtained with the simulations exhibited excellent agreement against the experiments. The simulations showed that this type of cavitation device can reduce the reaction time of the overall process as a result of the fast reaction times found in the regions where the bubbles collapse.

The PBM and CFD approaches examined in this sub-section have shown that higher reaction rates and better control of particle size can be achieved by improving the mixing efficiency in droplet-based microreactors or the bubble collapsing process in cavitating devices. Other factors that may affect the reaction rate are the reactor geometry and the initial concentration of the reactants. A strong limitation of these techniques is represented by the multiple physical parameters necessary to close the mathematical framework, which may include the reaction rates of nucleation and growth under different operating conditions or the interaction forces between the AgNPs. These physical parameters can be obtained from either experimental measurements or be estimated through MD simulations, paving the road for an expanded multi-scale framework for AgNPs synthesis. Despite the important strides mentioned, modelling the synthesis reactions of AgNPs in different types of reactors from a meso and macroscale perspective represents a new line of research that requires further investigation. In particular, a closer assessment of the validity of neglecting particle interaction phenomena through

agglomeration and breakup, and the consideration of the effect of stabilising agents, are needed for better predictions of the PSD.

6. Microfluidic synthesis of AgNPs: experiments and numerical simulations

Scaling down the reactor dimensions provides better control of the process of AgNPs synthesis and enables a low consumption and a high conversion of the reagents. Hence, the formation of undesired by-products and the waste produced are minimised, and the environmental impact is reduced [147]. By adjusting the supply of reagents for nucleation and growth, as well as varying the flow configuration, the size, shape and dispersity of particles can be controlled [148]. Specifically for the synthesis of AgNPs, the reduction stage is fast (less than 200ms, according to Polte, Tuaev [73]) and mixing of silver precursor and other reactants is a critical stage to establish uniform reaction conditions.

Continuous-flow [149] and drop-based production [150] are two of the main operational settings reported for microfluidic synthesis. Microfluidic flows are laminar, enabling a precise control of hydrodynamic conditions, with slow mixing being balanced by reduced path lengths of diffusion. Continuous-flow production involves a monophasic liquid system comprised of the reactants (i.e., the precursor, the reducing agent, and the stabilisers) in aqueous solutions, as depicted in **Figure 4 A**. Some of the main disadvantages of continuous flow microfluidic reactors are related to the classic laminar parabolic flow profile formed in the channel. The velocity distribution thus formed consequently causes a distribution of fluid residence times and the no-slip condition at the channel wall can lead to particle deposition and fouling or blockage of the channel. Performance of continuous flow reactors can be improved by employing channels with twists and turns to promote mixing [151] or by droplet-based operations. In drop microfluidics, discrete droplets are produced and manipulated using immiscible segmented liquid-liquid multiphase flows inside the microchannels. One of the liquid phases corresponds to an aqueous solution of the reactants and the other to an inert oil phase that carries the droplets through the channel, as shown in **Figure 4** B-D. A summary of relevant experimental studies on synthesis of AgNPs using microfluidic technology is presented in **Table 3.**

Drop-based synthesis is usually comprised of three general stages: drop formation, mixing of the reactants within the drop, and chemical reactions resulting in the formation of AgNPs. Two primary operational settings for drop-based synthesis are identified in the literature, one in which the reactants are brought together during the drop formation step (e.g., **Figure 4**), and one in which the reactants are initially in separate droplets that collide in the channel to initiate the mixing process and trigger the reactions. Several parameters determine the successful coalescence of drops, including the balance between the viscous, capillary, and inertial forces, the geometry of the channel, and the presence of surfactants [152]. The upcoming sub-sections explore drop formation and mixing in microfluidic devices. Experimental aspects of these topics have been discussed in numerous review papers (see for example Seemann, Brinkmann [153]), thus, mostly numerical and computational results are included.

6.1. Microfluidic drop formation

Drop formation and coalescence in microfluidic devices are well studied from both experimental and numerical perspectives. The drops can be formed using cross-flow (mostly variations of a T-junction), flow-focusing, and co-flow geometries [154] (**Figure 4** B-D, respectively) in two main regimes: squeezing/dripping (**Figure 4** E) and jetting (**Figure 4** F), with most monodisperse drops being formed in the dripping regime [155]. Therefore, the dripping regime appears to be the most suitable to produce drops in microfluidic reactors.

The drop size depends on the interfacial tension at the time of drop formation and the viscosity ratio between continuous and dispersed phases and can be easily adjusted by manipulating the flow rates of the phases: an increase in the dispersed to continuous flow rate ratio results in an increase of the drop size. (*cf.* **Figure 4** I and J). The range of flow rates of the continuous and dispersed phases ensuring fast and reliable drop formation in the dripping regime with required optimal drop size can be found experimentally, but it can also be predicted using numerical simulations, reducing demand in materials, experimental work time, and waste. Moreover, numerical simulations can provide further relevant information about the system. For example, simulations can describe the flow structures inside the forming drop responsible for the initial mixing of the reactants if they are all added simultaneously on the stage of drop formation (**Figure 4** K).

The computational literature pertaining drop formation in microchannels has been concerned mostly with the prediction of characteristics related to the flow regime of the dispersed phase, such as droplet size, shape, and frequency, and understanding the hydrodynamic mechanisms behind each regime. The central computational challenge for simulating this type of system relies on the correct treatment of the two-phase flow and attaining a well-defined interface. The two most common frameworks found in the literature are CFD-based VOF and level-set. Li, Li [156] investigated the drop formation process in a T-junction microchannel (**Figure 4** B) through VOF-based 3-D simulations in the commercial software ANSYS Fluent. Detailed analyses were provided regarding the local pressure and shear forces that compete against the interfacial tension prior to the moment of droplet pinch-off at the junction. It was found that, locally, variations in the pressure and velocity fields decrease with the flow rate of the continuous phase, generating shear stresses in the interface that drive the breakup process. It was also shown that pressure variations exist within the droplet itself, confirming the results of Sivasamy, Wong [157].

Table 3: Experimental investigations on microfluidic synthesis of AgNPs.

Silver Precursor	Reducing and stabilising agent or other reagents	Microfluidic type	Flow rates of continuous and dispersed phases	Size(nm)	References
$AgNO_3$	Borane dimethylamine (DMAB)/PVA and tween 80	Drop-based microfluidics: Two phase flow system	Continuous phase/ oil flow rate: 5 mL/h Dispersed phase/water or reagent flow rate: 1mL/h	2.5±0.5 nm	[158]
$AgNO_3$	Tannic acid/trisodium citrate	Drop-based microfluidics: Y junction with straight and serpentines channels	Continuous phase/oil flow rate:60 and 80 µL/h. Dispersed phase/ reactant flow:16 and 32µL/h.	16/60 µL/h→~16.3 nm 16/80 µL/h→ ~12.8 nm 32/60 µL/h→~20.7 nm 32/80 µL/h→~22.3 nm	[159]
$C_3AgF_5O_2$ (silver pentafluoro propionate)	Trioctylamine and isoamyl ether at 100-140 ℃	Continuous flow tubular microreactor	0.08-0.7 mL/min	0.08 mL/min→8.7±0.9 nm 0.6 mL/min→ NPs varied between 3 and 12 nm	[160]
$AgNO_3$	$NaBH_4$/trisodium citrate	Co-axial microfluidic reactor	1, 2, 8 and 14 mL/min	1mL/min →3.1±1.6 nm, 2mL/min →3.3±2.2 nm, 8mL/min →5.6±2.7 nm and 14 mL/min →5.4±3.4 nm	[161]

$AgBF_4$	1-Butyl-3-methylimidazolium borohydride (BMIM-BH_4)	Drop-based microfluidics: Multiple inlet T-junction device	Continuous phase/oil flow rate: 10 mL/h Dispersed phase/ reagent flow rates: 0.5 mL/h	3.73±0.77 nm	[162]
$AgNO_3$	Glucose/PVP	Piezoelectric actuated three phase flow pulsating mixing device	Inlets flow rate: 3.5 mL/min	29.11±3.98 nm	[163]
$AgNO_3$	$NaBH_4$/PVP and EDTA as complexing agent	Drop-based microfluidics: T-junction device	10-30 mL/h for both continuous phase/oil stream and dispersed phase/aqueous stream	10 mL/h→4.9±1.2 nm 30 mL/h→7.6±1.8 nm	[164]

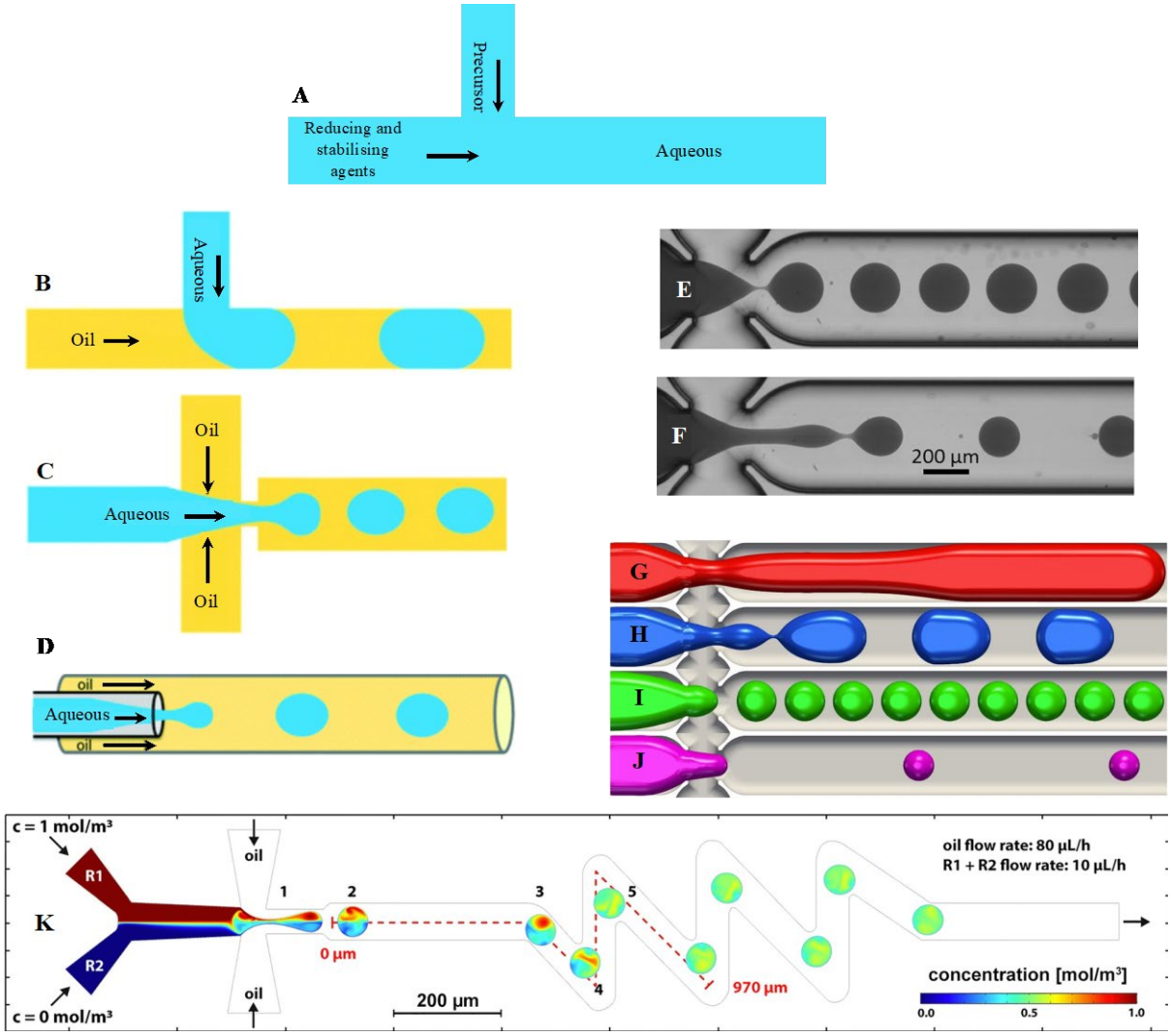

Figure 4: Schematic illustration of microfluidic synthesis in A) continuous-flow operation and B – D) drop-based operation for different channel configurations: B) T-junction geometry (cross-flow), C) flow focusing geometry and D) co-flow geometry [150]. Experimental results on drop formation in a flow-focusing device: E) dripping regime and F) jetting regime [165]. Numerical simulations for flow regimes in the same device as presented in E and F: G) threading regime without drop formation, H) large drops formed by coalescence events at the junction and I – J) drop formation in dripping regime at a flow rate ratio of dispersed and continuous phase of 1 (I) and 0.125 (J) [166]. K) formation of a complex drop from two reactant streams in a flow-focusing device and further mixing of reactants in serpentine channel. Concentration colour scale corresponds to the concentration of a model tracer. A value of 0.5 mol/m^3 corresponds to a well-mixed stage [159]

A VOF-based approach with smoothing operations to simulate the droplet formation process in a T-junction microchannel was suggested by Soh, Yeoh [167]. By comparing the length of the droplets predicted by the simulations to those of the experiments of Garstecki, Fuerstman [168] for different flow rates, Soh, Yeoh [167] demonstrated that the smoothing operations provide a more realistic

depiction of the system than the standard VOF model. From the simulations, Soh, Yeoh [167] described and analysed in detail the velocity fields that developed during the different stages of droplet formation for different flow rates of the dispersed phase and constant capillary number, $Ca_c = \mu_c U_c/\sigma$, of the continuous phase (μ_c and U_c represent the viscosity and velocity of the continuous phase, respectively, and σ the interfacial tension). It was found that important recirculation zones form near the tail of the droplet when the pinch-off point occurs similar to those found in the study of Kahouadji, Nowak [166]. This recirculation can be important for reactant premixing in the configuration shown in **Figure 4** K.

Recently, Filimonov, Wu [169] tested and proposed a series of measures in order to speed up VOF-based CFD simulations of droplet formation in a cross-junction configuration. The CFD simulations incorporated the effects of the surface tension between the liquid phases as well as the liquid-liquid-wall interaction through the specification of a contact angle. Their predictions were validated against the experiments of Wu, Cao [170] which obtained droplet and water slug lengths under different flow rates. It was found that higher contact angles were associated with smaller droplets and slugs (higher frequency of droplet formation). The most relevant measures proposed by Filimonov, Wu [169] to increase the simulation efficiency are:

1. Applying one symmetry plane in the horizontal direction and one in the cross-section of the channel.

2. Imposing developed velocity profiles at the inlets. These velocity profiles can be obtained from steady-state one-phase simulations in the microchannel.

3. Avoiding unnecessary cell refinement at the inlet regions of the channel given that the liquid-liquid surface tension has virtually no effect on those regions.

Wu, Liu [171] investigated droplet formation in co-flow and flow-focusing microchannels through 2-D axisymmetric CFD simulations based on the VOF approach with CSF. The effects of Ca of the continuous phase and the geometry of the microchannels on the flow regime, drop size, and frequency of formation were explored. More specifically, the inlet velocity of the continuous phase was incremented to observe the transition between the dripping and jetting regimes for both microchannels.

For the flow-focusing channel, the length, and the radius of the focusing orifice were modified, and their influence on the aforementioned parameters was analysed. In the case of the flow-focusing channel, the transition between the dripping and jetting regimes occurs at lower Ca, indicating that the focusing orifice accentuates the effects of the continuous phase hydrodynamics. It was also observed that, under the same operating conditions, the droplets formed in flow-focusing channels tend to be smaller and with higher polydispersity in terms of size than those formed in co-flow channels.

A level-set investigation as conducted by Kahouadji, Nowak [166]. In this study, the authors simulated the dynamics of a 3-D two-phase flow in a flow-focusing microfluidic channel commercially available from Dolomite (**Figure 4** E-J). The level-set method with interface tracking was employed to treat the multiphase system and avoid the typical numerical instabilities that arise in surface tension-driven flows. Kahouadji, Nowak [166] showed that numerical simulations can account for various flow regimes also observed in experiments (**Figure 4** G-J). Details of the drop formation process were analysed, such as the period of formation and separation length between drops and the complex velocity fields and recirculation patterns. It was found that clear vortex structures emerge in both phases right before the drop pinch-off, which is a phenomenon that had been previously observed for the dispersed phase using μ-PIV experimental techniques [172].

For future work, Kahouadji, Nowak [166] highlighted the importance of a detailed analysis of the droplet formation mechanism in microchannels in the presence of a surface-active agent. Considering that the synthesis processes of AgNPs typically involve the use of a stabiliser, additional information about the influence of a surfactant on the shape of the droplet and the flow patterns formed in the channel would greatly enrich the study of the synthesis of AgNPs in droplet-based microfluidics.

6.2. Dynamics of droplet mixing in droplet-based microfluidic devices

It has been widely demonstrated experimentally that the mixing process within droplets is an essential stage of the process of AgNP synthesis in droplet-based microreactors since it has a significant influence on the properties of the final product obtained (see Kašpar, Koyuncu [173] and references therein). Consequently, a significant effort has been made to understand how the mixing process occurs within

the droplets, and how different factors, mainly the channel geometry, the flowrates of the phases, and the capillary number, could impact the mixing efficiency.

Similar to drop formation (detailed in the last sub-section), the problem of mixing within droplets has mostly been tackled computationally through variations of the VOF and level-set methods. To account for mixing, the two-phase framework is usually coupled with an additional convection-diffusion equation for either the mixing fraction for the kth mixture (f_k), as seen in Wang, Wang [174], or a model tracer, as seen in Sarrazin, Loubière [175]. **Eq. (8)** depicts the mathematical description of this transport equation for f_k:

$$\frac{\partial(\rho f_k)}{\partial t} + \nabla \cdot (\rho \mathbf{u} f_k) = D\nabla^2 f_k, \qquad \textbf{(8)}$$

where D is a diffusion coefficient, and ρ is the fluid density. The quantification of the degree of species homogeneity within the drops has usually been achieved through the estimation the mixing efficiency, whose mathematical expression is shown in **Eq. (9)**. In this equation, c_i is the concentration distribution or mixing fraction within the drop at a certain time/position, c_0 is the concentration distribution or mixing fraction at the initial stage (before mixing), and c_∞ is the concentration distribution or mixing fraction of the perfect mixture. With this definition, $m_e = 0$ corresponds to full segregation of the reactants and $m_e = 1$ to a perfectly homogeneous mixture:

$$m_e = 1 - \frac{\int_A |c_i - c_\infty| dA}{\int_A |c_0 - c_\infty| dA}. \qquad \textbf{(9)}$$

An example this approach is found in Sarrazin, Loubière [175], who were among the first to use a VOF method without computationally expensive interface reconstruction to simulate a 3-D droplet in straight rectangular microchannels. Molecular diffusion was assumed to be negligible in comparison to convection in the transport equation for the model tracer. The velocity profile results from the simulations were compared against PIV experimental measurements. It was observed that two zones of symmetric recirculating flow developed in the droplet without significant mixing between the two zones. This indicates that, if the reactants are introduced on the stage of drop formation, as shown in **Figure 4** K, the convective mixing of these reactants in straight channels will be negligible, hindering

the synthesis reactions. To enhance the mixing intensity, serpentine channels have been proposed as a promising solution to this problem [176].

Mixing in serpentine channels was investigated in the comprehensive study of Kašpar, Koyuncu [173] (results shown in **Figure 4** K). In this experimental and CFD study, AgNPs were prepared by a reduction reaction of silver nitrate with tannic acid in the presence of trisodium citrate (stabilising agent). The flows of the reactants, the stabilising agent, and the continuous phase (mineral oil) met at a junction where the aqueous droplets formed and then travelled through a meandering channel. In contrast to most studies of this type, the CFD simulations were not based on a VOF approach but on a field-based level set method in which a conservation equation for the level set function is added to the model. A computational model tracer was added to the simulations in order to track the mixing process inside the droplet with the same approach mentioned previously.

The experimental and CFD results of Kašpar, Koyuncu [173] provided important insights into the droplet formation and mixing process. In particular, the mixing analyses made in this study confirmed the discoveries of previous authors regarding the effects of channel bends in the mixing efficiency of the droplets. The simulations showed that, after 40ms of operating time, a droplet flowing through a straight channel would only reach a mixing efficiency of 67%, while a droplet flowing through a meandering channel would reach a mixing efficiency of about 88% at the same flow rates (compare the poor mixing exhibited by the droplets in the straight sections of the channel in points 1-3 to the high mixing quality in meandering sections on points 4-5 of **Figure 4** K).

Similar to Kašpar, Koyuncu [173], Wang, Wang [174] simulated a droplet-based mixing process in a serpentine microchannel, but with a VOF approach. This study provided additional insights into the mixing process by estimating the circulation period within a droplet. To achieve this, the authors used a Discrete Phase Model (DPM), in which tracer particles were placed at the centre of a droplet, and their movement was tracked. The time needed for a particle to travel one period within the droplet was taken as the circulation period. In agreement with previous studies on the matter, Wang, Wang [174] attribute the improved mixing process of serpentine channels compared to straight channels to the asymmetrical recirculation regions that form in the bends of the channels.

Wu, De Varine Bohan [177] investigated the effect of the curvature and torsion of a helical microreactor and the flow rate on the particle size and polydispersity of AgNPs formed without the presence of a capping agent. The CFD simulations were run using the commercial software ANSYS Fluent with a similar DPM as the one used in Wang, Wang [174]. Through combined CFD-experimental approaches, Wu, De Varine Bohan [177] demonstrated that the secondary flows that arise when the droplet reaches a bend in the microreactor also promote nucleation. It was also demonstrated that decreasing the helix's diameter and increasing the total flow rate led to smaller average particle sizes.

Better convective mixing is expected if the reaction is triggered by coalescence of two drops following each other [175]. This conclusion is supported by experimental studies, which also show that, for drops having initially different interfacial tensions, mixing depends on the drop order, as seen in **Figure 5** [178]. A comprehensive analysis of droplets following each other in a planar serpentine microchannel was made by Tung, Li [179]. The CFD model consisted of a VOF approach with a piecewise linear interface calculation (PLIC) for interface tracking. The surface tension forces in the momentum equation were represented with a CSF model. Mixing was modelled by means of a conservation equation for the mixture fraction (see **Eq. (8)**) and the mixing index (see **Eq. (9)**).

The velocity profiles across the droplet were compared to μ-PIV measurements. The analyses provided by Tung, Li [179] are in agreement with previous experimental works (see Kovalchuk, Reichow [178]). These analyses show that, in the case of straight channels, recirculating flows are formed in each half of the drop (**Figure 5** A-B). In contrast, when the drop moves through a winding section, it undergoes stretching, folding, and reorienting processes, creating chaotic recirculating flows that promote further mixing of the droplet halves, **Figure 5** C. The large difference in the mixing index for drop moving in straight and winding channel in the case when 2 solutions are introduced symmetrically along the flow direction is shown in **Figure 5** D.

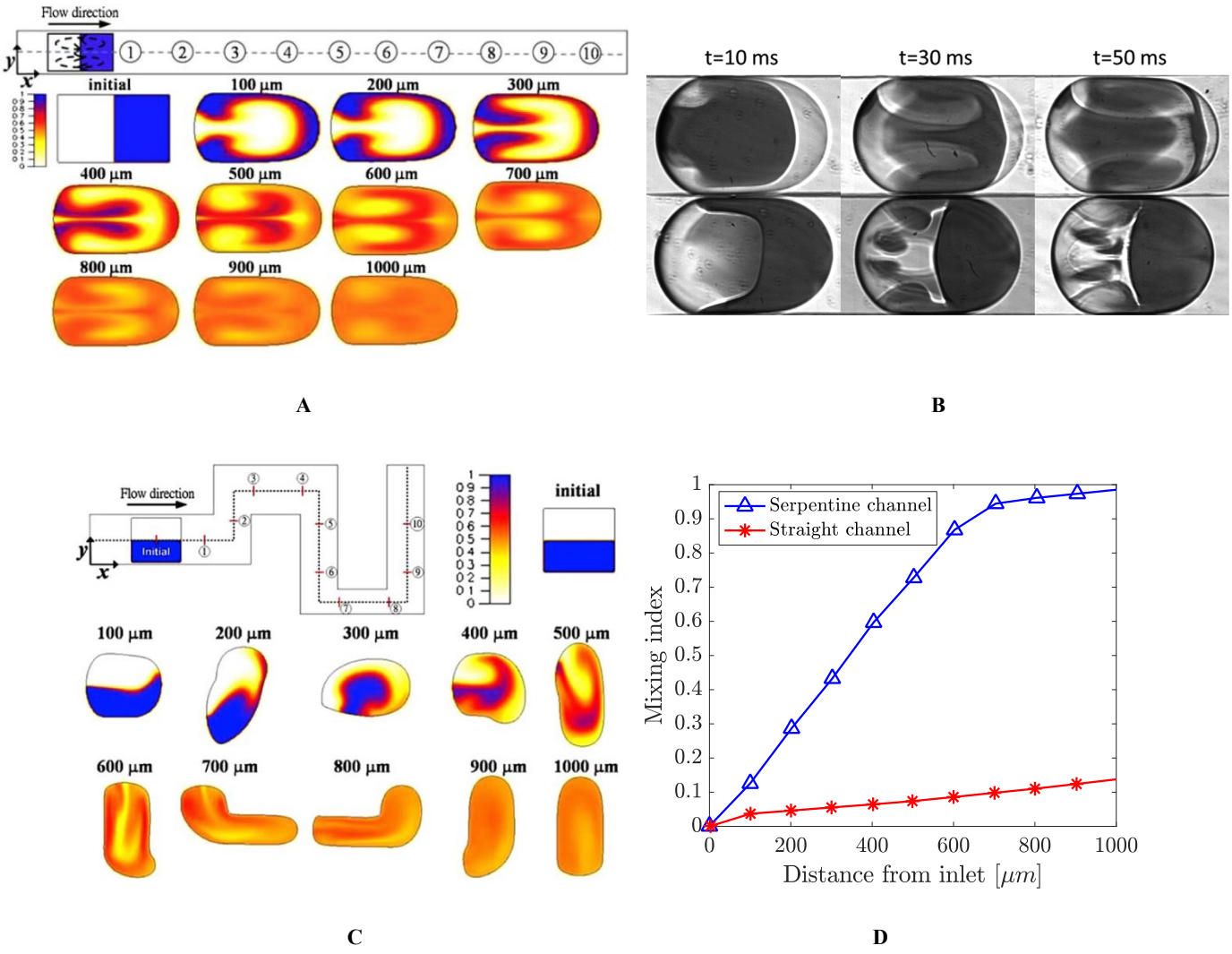

Figure 5: Mixing in a straight vs. a serpentine channel: A – straight channel for the case when two solutions are aligned sequentially along the flow direction, numerical results; B – the same as A, experimental results, top row – the front part has smaller interfacial tension, bottom row – the front part has larger interfacial tension; C – mixing in straight and winding channel for the case when solutions are aligned parallel along the flow direction, numerical results; D – difference in mixing index for the straight and winding channel for the case when solutions are aligned parallel along the flow direction, numerical results. Results from the simulations of Tung, Li [179] and experiments of Kovalchuk, Reichow [178]Results from the simulations of Tung, Li [179] and experiments of Kovalchuk, Reichow [178].

Table 4 contains a summary of the most relevant computational studies available in the literature about passive droplet-mixing in microchannels. Some characteristics of numerical methods used, the specific system studied, and the most important results are included. CFD-based simulations have confirmed and expanded previous experimental observations about the increased mixing efficiency of serpentine channels in comparison to straight channels. In particular, the quantification of the mixing index and

the possibility of 3-D visualisation of the flow field have led to discover that the poor mixing exhibited in straight microchannels can be ascribed to the two symmetric recirculation zones that develop within the droplet. In contrast, when the droplet encounters twists and bends in serpentine channels, unsymmetric shear forces significantly deform the droplet, leading to chaotic recirculation zones that promote mixing. Such detailed insights about the flow fields of the systems have been achieved by leveraging the advantages of VOF and level-set methods to treat the two-phase flow. Despite the important advances mentioned, a few key aspects remain unresolved. Notably, a comparison of the performance and computational expense of these two-phase frameworks (VOF and level-set) within the context of AgNP synthesis in microchannels is still largely missing from the literature. Furthermore, a systematic examination of whether the observations of the flow fields in straight vs. serpentine channels remain valid for a span of different dimensionless parameters, such as Ca, and different shapes of the cross-section area of the microchannel would greatly benefit the field.

Table 4: Summary of the most relevant CFD-related studies about droplet-mixing in microchannels. All fluids involved in all studies listed were assumed to be Newtonian and their flows incompressible

Study	Junction/inlets	Channel geometry	Phases/species	Computational method	Software	Simulation domain	Parameters analysed
Muradoglu and Stone [180]	Droplets placed instantaneously at the inlet with the continuous phase. Tracers placed at the top half of the droplets	Serpentine channel	Not stated	Interface tracking with passive tracers	Not stated	2-D	Influence of the capillary number, ratio between the phases' viscosities and Reynolds number on the mixing efficiency.
Sarrazin, Loubière [175]	Droplets placed instantaneously at the inlet with the continuous phase. Periodic boundary conditions applied to the inlet and outlet to study a single droplet	Rectangular straight channel	Continuous phase: silicone oil Dispersed phase: water	VOF without interface reconstruction. Inclusion of passive tracers	Open-source code: JADIM	3-D. Simulated domain corresponds to one fourth of the channel	1. Velocity fields in the slugs/droplets. 2. Trajectory of the tracer within a droplet to observe the mixing process.
Tung, Li [179]	Droplets placed instantaneously at the inlet with the continuous phase.	Planar serpentine channel	Continuous phase: silicone oil Dispersed phase: water and Tween 20	VOF with interface capturing (PLIC). CSF model for surface tension. Inclusion of passive tracers	Commercial code: CFD-ACE+	2-D	1. Velocity fields in the droplets. 2. Mixing index within droplets travelling in different sections of the channel. 3. Maximum vorticity difference within droplets. 4. Droplet deformation in the channel bends.

CHANDORKAR and PALIT [181]	T-Junction	Straight and Single-bend channel	Continuous phase: perfluorocarbon Dispersed phase: water	VOF. Interface capturing not mentioned. Inclusion of passive tracers	Commercial code: FLOW-3D	3-D	1. Influence of the phases' flow rates on droplet frequency and droplet/slug length. 2. Evolution of the profiles of the tracer's concentration in the droplet.
Wang, Wang [174]	Three-way junction	Serpentine channel	Continuous phase: oil Dispersed phase: water	VOF with interface capturing (PLIC). CSF model for surface tension. Inclusion of passive tracers. DPM included to track the trajectory of a model particle within a droplet	Commercial code: ANSYS Fluent	3-D	1. Droplet deformation in the channel bends. 2. Influence of the flow rate of the dispersed phase on the mixing index. 3. Detailed velocity profiles to demonstrate asymmetrical mixing in meandering channels. 4. Influence of the droplet size in the circulation period of the tracking particles
Özkan and Erdem [182]	T-Junction	Straight and sinusoidal channel	Not stated	Field-based level set method. DPM included to track the trajectory of a model particle within a droplet	Commercial code: COMSOL Multiphysics	3-D. Simulated domain corresponds to half of the channel with a symmetry condition	Influence of the cross-sectional area of the microchannel on hydraulic mixing.
Filatov, Belousov [183]	Variations of a Y-junction	Straight channels	Continuous phase: oil Dispersed phase: water	Field-based level set method	Commercial code: COMSOL Multiphysics	2-D	Influence of the capillary number on the droplet length and mixing index for different junction geometries.

Yang, Li [184]	Three-way junction	Straight and Convergent - divergent sinusoidal channel	Continuous phase: oil Dispersed phase: water	Field-based level set method. Inclusion of passive tracers	Commercial code: COMSOL Multiphysics	Not stated	1. Influence of the flow rate of the continuous phase on the mixing index. 2. Evolution of the velocity and concentration profiles throughout the channel. 3. Mixing index reached with a proposed sinusoidal geometry.
Wu, De Varine Bohan [177]	Droplets placed instantaneously at the inlet with the continuous phase.	Straight and helical channels	Not stated	Treatment of multiphase flow not stated. DPM included to track the trajectory of a model particle within a droplet	Commercial code: ANSYS Fluent	Not stated	Influence of the dimensionless curvature and torsion of the helical channel on the droplet size.
Kašpar, Koyuncu [173]	Double Y-junction	Straight and serpentine channel	Continuous phase: mineral oil Dispersed phase: silver nitrate, tannic acid, and trisodium citrate solutions	Field-based level set method. Inclusion of passive tracers	Commercial code: COMSOL Multiphysics	3-D and 2-D	1. Influence of the capillary number and the flow rates on the flow pattern developed. 2. Influence of the flow rates on the droplet size and length, and the separating distance between droplets. 3. Evolution of the mixing efficiency in straight and serpentine channels.

7. Conclusions and perspectives

This review paper examines the formation process of AgNPs, their nucleation and growth mechanisms, and their properties with an extensive look at microfluidic technology and computational modelling as emerging approaches to be further exploited for their sustainable production. The available experimental literature reveals that chemical reduction is the most commonly used method to produce AgNPs. Microfluidic devices and their possible operational configurations, such as droplet-based and continuous flow, enable precise control of the reaction environment and reduce the polydispersity of AgNPs. Operating conditions, such as type and concentration of reagents, temperature control, pH of the solution, and mixing, are crucial parameters for controlling the size of the nanoparticles. The possibility to control size and other morphological characteristics of AgNPs is of great importance for their catalytic, optical, and electrical properties and possible new applications. Kinetic aspects and mechanisms have been studied through Finke-Watzky two-step mechanism, which can be used to describe the autocatalytic nature of AgNPs formation, but a model which includes the process of hydrodynamics is needed to obtain a more detailed mechanistic description.

From the computational side, MD simulations have been shown to be particularly useful in the field of AgNPs to understand the interaction between these nanoparticles and other entities, such as capping and structure-directing agents. These interactions explain how NPs with shapes tailored to specific applications can be obtained through the selection of a stabilising agent with precise characteristics in the synthesis process. Meso- and macroscopic aspects have been studied numerically mostly via coupled PBM-CFD simulations in both traditional batch-like reactors and microfluidic channels. The representation of the particle population through the mesoscale lens given by PBM provides a comprehensive description of the PSD and the average particle size, allowing to consider aspects such as particle nucleation and growth together with hydrodynamic aspects, such as mixing, through CFD. As a starting point for future research, a rigorous assessment of the importance of particle-particle interactions is deemed necessary to determine whether agglomeration and breakup phenomena should be included in the PBE. The current literature is also severely lacking investigations in which the major

stages of synthesis in microchannels (droplet formation and collision, mixing within droplets, and synthesis reactions) are simulated simultaneously under different conditions of Ca and channel geometry. Given that the phenomena occurring in these three stages interact with one another, the proposal of a computational method related to PBM and CFD that couples the three stages is of vital interest in the field. Out of these three stages, the last stage in particular (synthesis reactions) has taken the least prominent role in the literature, which the authors believe could be a starting point for further research. Another crucial yet unexplored topic corresponds to the possible effects of the presence of surface-active capping/stabilising agents in meso- and macroscale properties, such as the resulting droplet size, coalescence probability and mixing. The potential analyses produced from these topics would be a good complement to the aforementioned advancements from the molecular scale.

In addition to physics-driven computational models, data-driven and data-assisted models have risen in the past few years as powerful and innovative tools to investigate multiple aspects related to AgNPs at a significantly lower computational cost. Most research studies have been devoted to identifying non-trivial connections between operating conditions and characteristics of the final product to either predict the final particle size for a given process, or to obtain AgNPs with entirely new properties. Despite these advances, the present-day data-driven models can only provide limited information about the underlying physics behind the synthesis process, and the accuracy of these models is largely tied to the amount and quality of data used for training, testing, and validation. The advent of improved techniques, together with high-throughput experimental methods, such as microfluidic synthesis, illustrate a route for novel frameworks in which information is systematically exchanged between experiments, physics-based, and data-driven computational models. The authors believe that such framework could greatly advance the topic of AgNP synthesis as it would provide tools of analysis able to make connections between physical phenomena at different scales, and properties of interest for different applications.

Acknowledgments

The authors gratefully acknowledge the support from the Engineering & Physical Sciences Research Council, UK, through the PREMIERE Programme Grant EP/T000414/1. KN PhD studentship is funded

by University of Birmingham. PP PhD studentship is funded by Imperial College London and the Colombian Ministry of Science, Technology and Innovation (MINCIENCIAS).

References

1. Newswire, P.R., *Silver Nanoparticles Market to Garner $4.1 Billion, Globally, By 2027 at 15.7% CAGR, Says Allied Market Research*, in *AlliedMarketResearch*. 2020, Y.
2. Vazquez-Muñoz, R., et al., *Enhancement of antibiotics antimicrobial activity due to the silver nanoparticles impact on the cell membrane.* PLoS One, 2019. **14**(11).
3. Lu, L., et al., *Silver nanoparticles inhibit hepatitis B virus replication.* Antivir Ther, 2008. **13**(2): p. 253-62.
4. Elechiguerra, J.L., et al., *Interaction of silver nanoparticles with HIV-1.* Journal of Nanobiotechnology, 2005. **3**(1): p. 6.
5. Wei, F., et al., *A novel strategy for water disinfection with a AgNPs/gelatin sponge filter.* Environmental Science and Pollution Research, 2018. **25**(20): p. 19480-19487.
6. Wu, Z., et al., *Multifunctional chitosan-based coating with liposomes containing laurel essential oils and nanosilver for pork preservation.* Food Chemistry, 2019. **295**: p. 16-25.
7. Ballottin, D., et al., *Antimicrobial textiles: Biogenic silver nanoparticles against Candida and Xanthomonas.* Materials Science and Engineering: C, 2017. **75**: p. 582-589.
8. Szczepańska, E., et al., *Synthesis of silver nanoparticles in context of their cytotoxicity, antibacterial activities, skin penetration and application in skincare products.* Supramolecular Chemistry, 2020. **32**(3): p. 207-221.
9. Parveen, A., et al., *In vivo efficacy of biocompatible silver nanoparticles cream for empirical wound healing.* J Tissue Viability, 2018. **27**(4): p. 257-261.
10. Chutrakulwong, F., et al., *In Situ Deposition of Green Silver Nanoparticles on Urinary Catheters under Photo-Irradiation for Antibacterial Properties.* Processes, 2020. **8**(12): p. 1630.
11. Dantas, K.N.M., et al., *Antimycotic nail polish based on humic acid-coated silver nanoparticles for onychomycosis.* Journal of Chemical Technology & Biotechnology, 2021. **96**(8): p. 2208-2218.
12. Syafiuddin, A., et al., *Sticky silver nanoparticles and surface coatings of different textile fabrics stabilised by Muntingia calabura leaf extract.* SN Applied Sciences, 2020. **2**(4): p. 733.
13. Noronha, V.T., et al., *Silver nanoparticles in dentistry.* Dent Mater, 2017. **33**(10): p. 1110-1126.
14. Paul, S., et al., *Biochemical estimation of Moringa oleifera leaf extract for synthesis of silver nanoparticle mediated drug delivery system.* Journal of Plant Biochemistry and Biotechnology, 2020. **29**(1): p. 86-93.
15. Loiseau, A., et al., *Silver-Based Plasmonic Nanoparticles for and Their Use in Biosensing.* Biosensors (Basel), 2019. **9**(2).
16. Magdassi, S., et al., *Triggering the Sintering of Silver Nanoparticles at Room Temperature.* ACS Nano, 2010. **4**(4): p. 1943-1948.

17. Camargo, J.R., et al., *Development of conductive inks for electrochemical sensors and biosensors.* Microchemical Journal, 2021. **164**: p. 105998.
18. Camargo, J.R., et al., *Waterproof paper as a new substrate to construct a disposable sensor for the electrochemical determination of paracetamol and melatonin.* Talanta, 2020. **208**: p. 120458.
19. Bariya, M., et al., *Roll-to-Roll Gravure Printed Electrochemical Sensors for Wearable and Medical Devices.* ACS Nano, 2018. **12**(7): p. 6978-6987.
20. Dong, X.-Y., et al., *Nanosilver as a new generation of silver catalysts in organic transformations for efficient synthesis of fine chemicals.* Catalysis Science & Technology, 2015. **5**(5): p. 2554-2574.
21. Bogireddy, N.K.R., H.A. Kiran Kumar, and B.K. Mandal, *Biofabricated silver nanoparticles as green catalyst in the degradation of different textile dyes.* Journal of Environmental Chemical Engineering, 2016. **4**(1): p. 56-64.
22. Huff, C., J.M. Long, and T.M. Abdel-Fattah, *Beta-Cyclodextrin-Assisted Synthesis of Silver Nanoparticle Network and Its Application in a Hydrogen Generation Reaction.* Catalysts, 2020. **10**(9): p. 1014.
23. Krajczewski, J., K. Kołątaj, and A. Kudelski, *Plasmonic nanoparticles in chemical analysis.* RSC Advances, 2017. **7**(28): p. 17559-17576.
24. Song, J., et al., *Colorimetric detection of melamine in pretreated milk using silver nanoparticles functionalized with sulfanilic acid.* Food Control, 2015. **50**: p. 356-361.
25. Alzahrani, E., *Colorimetric Detection Based on Localized Surface Plasmon Resonance Optical Characteristics for Sensing of Mercury Using Green-Synthesized Silver Nanoparticles.* Journal of Analytical Methods in Chemistry, 2020. **2020**: p. 6026312.
26. Yen, C.W., et al., *Multicolored silver nanoparticles for multiplexed disease diagnostics: distinguishing dengue, yellow fever, and Ebola viruses.* Lab Chip, 2015. **15**(7): p. 1638-41.
27. Liu, R., et al., *In situ decoration of plasmonic silver nanoparticles on poly(vinylidene fluoride) membrane for versatile SERS detection.* New Journal of Chemistry, 2019. **43**(18): p. 6965-6972.
28. Tzeng, Y. and B.-Y. Lin, *Silver-Based SERS Pico-Molar Adenine Sensor.* Biosensors, 2020. **10**(9): p. 122.
29. Liu, H., et al., *Paper-based sandwich type SERS sensor based on silver nanoparticles and biomimetic recognizer.* Sensors and Actuators B: Chemical, 2020. **313**: p. 127989.
30. Lee, S.H. and B.H. Jun, *Silver nanoparticles: Synthesis and application for nanomedicine*, in *International Journal of Molecular Sciences*. 2019, MDPI AG. p. 865.
31. Reverberi, A.P., et al., *Green Synthesis of Silver Nanoparticles by Low-Energy Wet Bead Milling of Metal Spheres.* Materials, 2020. **13**(1): p. 63.
32. Quintero-Quiroz, C., et al., *Optimization of silver nanoparticle synthesis by chemical reduction and evaluation of its antimicrobial and toxic activity.* Biomaterials Research, 2019. **23**(1): p. 27.
33. El-Khatib, A.M., et al., *Synthesize of Silver Nanoparticles by Arc Discharge Method Using Two Different Rotational Electrode Shapes.* Journal of Cluster Science, 2018. **29**(6): p. 1169-1175.
34. Siddiqi, K.S., A. Husen, and R.A.K. Rao, *A review on biosynthesis of silver nanoparticles and their biocidal properties.* Journal of Nanobiotechnology, 2018. **16**(1): p. 14.

35. Zahoor, M., et al., *A Review on Silver Nanoparticles: Classification, Various Methods of Synthesis, and Their Potential Roles in Biomedical Applications and Water Treatment.* Water, 2021. **13**(16): p. 2216.
36. Yaqoob, A.A., K. Umar, and M.N.M. Ibrahim, *Silver nanoparticles: various methods of synthesis, size affecting factors and their potential applications–a review.* Applied Nanoscience, 2020. **10**(5): p. 1369-1378.
37. Winkler, D.A., *Role of Artificial Intelligence and Machine Learning in Nanosafety.* Small, 2020.
38. Watzky, M.A. and R.G. Finke, *Transition Metal Nanocluster Formation Kinetic and Mechanistic Studies. A New Mechanism When Hydrogen Is the Reductant: Slow, Continuous Nucleation and Fast Autocatalytic Surface Growth.* Journal of the American Chemical Society, 1997. **119**(43): p. 10382-10400.
39. LaMer, V.K. and R.H. Dinegar, *Theory, Production and Mechanism of Formation of Monodispersed Hydrosols.* Journal of the American Chemical Society, 1950. **72**(11): p. 4847-4854.
40. Lifshitz, I.M. and V.V. Slyozov, *The kinetics of precipitation from supersaturated solid solutions.* Journal of Physics and Chemistry of Solids, 1961. **19**(1): p. 35-50.
41. Manikprabhu, D. and K. Lingappa, *Microwave Assisted Rapid and Green Synthesis of Silver Nanoparticles Using a Pigment Produced by Streptomyces coelicolor klmp33.* Bioinorganic Chemistry and Applications, 2013. **2013**: p. 341798.
42. Roldán, M.V., N. Pellegri, and O. de Sanctis, *Electrochemical Method for Ag-PEG Nanoparticles Synthesis.* Journal of Nanoparticles, 2013. **2013**: p. 524150.
43. Nakano, M., T. Fujiwara, and N. Koga, *Thermal Decomposition of Silver Acetate: Physico-Geometrical Kinetic Features and Formation of Silver Nanoparticles.* The Journal of Physical Chemistry C, 2016. **120**(16): p. 8841-8854.
44. Navaladian, S., et al., *Thermal decomposition as route for silver nanoparticles.* Nanoscale Res Lett, 2006. **2**(1): p. 44-8.
45. Hosseinpour-Mashkani, S.M. and M. Ramezani, *Silver and silver oxide nanoparticles: Synthesis and characterization by thermal decomposition.* Materials Letters, 2014. **130**: p. 259-262.
46. Wani, I.A., et al., *Structural characterization and antimicrobial properties of silver nanoparticles prepared by inverse microemulsion method.* Colloids and Surfaces B: Biointerfaces, 2013. **101**: p. 243-250.
47. Zhang, W., X. Qiao, and J. Chen, *Formation of silver nanoparticles in SDS inverse microemulsions.* Materials Chemistry and Physics, 2008. **109**(2): p. 411-416.
48. Lee, K.J., et al., *Direct synthesis and inkjetting of silver nanocrystals toward printed electronics.* Nanotechnology, 2006. **17**(9): p. 2424-2428.
49. Li, K., et al., *Preparation of Spherical and Triangular Silver Nanoparticles by a Convenient Method.* Integrated Ferroelectrics, 2012. **136**(1): p. 9-14.
50. Kim, D., S. Jeong, and J. Moon, *Synthesis of silver nanoparticles using the polyol process and the influence of precursor injection.* Nanotechnology, 2006. **17**(16): p. 4019-4024.
51. Wang, H., et al., *Preparation of silver nanoparticles by chemical reduction method.* Colloids and Surfaces A: Physicochemical and Engineering Aspects, 2005. **256**(2): p. 111-115.
52. Khan, Z., et al., *Preparation and characterization of silver nanoparticles by chemical reduction method.* Colloids and Surfaces B: Biointerfaces, 2011. **82**(2): p. 513-517.
53. Aktara, M.N., et al., *The synthesis of thiol-stabilized silver nanoparticles and their application towards the nanomolar-level colorimetric recognition of glutathione.* New Journal of Chemistry, 2019. **43**(34): p. 13480-13490.

54. La Spina, R., et al., *Synthesis of Citrate-Stabilized Silver Nanoparticles Modified by Thermal and pH Preconditioned Tannic Acid.* Nanomaterials, 2020. **10**(10): p. 2031.
55. Thanh, N.T.K., N. Maclean, and S. Mahiddine, *Mechanisms of Nucleation and Growth of Nanoparticles in Solution.* Chemical Reviews, 2014. **114**(15): p. 7610-7630.
56. Nagarajan, R., *Nanoparticles: Building Blocks for Nanotechnology*, in *Nanoparticles: Synthesis, Stabilization, Passivation, and Functionalization*. 2008, American Chemical Society. p. 2-14.
57. Rivero, P.J., et al., *Effect of both protective and reducing agents in the synthesis of multicolor silver nanoparticles.* Nanoscale research letters, 2013. **8**(1): p. 101-101.
58. Ranoszek-Soliwoda, K., et al., *The role of tannic acid and sodium citrate in the synthesis of silver nanoparticles.* Journal of Nanoparticle Research, 2017. **19**(8): p. 273.
59. V. Goia, D. and E. Matijević, *Preparation of monodispersed metal particles.* New Journal of Chemistry, 1998. **22**(11): p. 1203-1215.
60. Van Hyning, D.L. and C.F. Zukoski, *Formation Mechanisms and Aggregation Behavior of Borohydride Reduced Silver Particles.* Langmuir, 1998. **14**(24): p. 7034-7046.
61. Wuithschick, M., et al., *Size-Controlled Synthesis of Colloidal Silver Nanoparticles Based on Mechanistic Understanding.* Chemistry of Materials, 2013. **25**(23): p. 4679-4689.
62. Glushko, V.N., et al., *Features of Obtaining Silver Nanoparticles in Non-Aqueos Media by Reduction of Silver Trifluoroacetate.* Oriental Journal of Chemistry, 2015. **31**(4): p. 2515-2520.
63. Halder, S., et al., *Size-Controlled Facile Synthesis of Silver Nanoparticles by Chemical Reduction Method and Analysis of Their Antibacterial Performance.* ChemistrySelect, 2021. **6**(36): p. 9714-9720.
64. Jana, N.R. and X. Peng, *Single-Phase and Gram-Scale Routes toward Nearly Monodisperse Au and Other Noble Metal Nanocrystals.* Journal of the American Chemical Society, 2003. **125**(47): p. 14280-14281.
65. Dung, C.T., et al., *Combination of 4-ATP Coated Silver Nanoparticles and Magnetic Fe3O4 Nanoparticles by Inverse Emulsion Method.* VNU Journal of Science: Mathematics - Physics, 2014. **30**(2).
66. Andrieux-Ledier, A., B. Tremblay, and A. Courty, *Synthesis of Silver Nanoparticles Using Different Silver Phosphine Precursors: Formation Mechanism and Size Control.* The Journal of Physical Chemistry C, 2013. **117**(28): p. 14850-14857.
67. Ge, L., et al., *Nanosilver particles in medical applications: synthesis, performance, and toxicity.* International journal of nanomedicine, 2014. **9**: p. 2399-2407.
68. Kathiravan, V., S. Ravi, and S. Ashokkumar, *Synthesis of silver nanoparticles from Melia dubia leaf extract and their in vitro anticancer activity.* Spectrochim Acta A Mol Biomol Spectrosc, 2014. **130**: p. 116-21.
69. Huang, J., et al., *Biosynthesis of silver and gold nanoparticles by novel sundriedCinnamomum camphoraleaf.* Nanotechnology, 2007. **18**(10): p. 105104.
70. Cruz, D., et al., *Preparation and physicochemical characterization of Ag nanoparticles biosynthesized by Lippia citriodora (Lemon Verbena).* Colloids and Surfaces B: Biointerfaces, 2010. **81**(1): p. 67-73.
71. Nadagouda, M.N. and R.S. Varma, *Green synthesis of silver and palladium nanoparticles at room temperature using coffee and tea extract.* Green Chemistry, 2008. **10**(8): p. 859-862.

72. Ahmad, S., et al., *Green nanotechnology: a review on green synthesis of silver nanoparticles - an ecofriendly approach.* Int J Nanomedicine, 2019. **14**: p. 5087-5107.
73. Polte, J., et al., *Formation Mechanism of Colloidal Silver Nanoparticles: Analogies and Differences to the Growth of Gold Nanoparticles.* ACS Nano, 2012. **6**(7): p. 5791-5802.
74. Xie, Y., R. Ye, and H. Liu, *Synthesis of silver nanoparticles in reverse micelles stabilized by natural biosurfactant.* Colloids and Surfaces A: Physicochemical and Engineering Aspects, 2006. **279**(1): p. 175-178.
75. Zhang, W., X. Qiao, and J. Chen, *Synthesis of nanosilver colloidal particles in water/oil microemulsion.* Colloids and Surfaces A: Physicochemical and Engineering Aspects, 2007. **299**(1): p. 22-28.
76. Lin, X.Z., X. Teng, and H. Yang, *Direct Synthesis of Narrowly Dispersed Silver Nanoparticles Using a Single-Source Precursor.* Langmuir, 2003. **19**(24): p. 10081-10085.
77. Chandhru, M., et al., *One-pot green route synthesis of silver nanoparticles from jack fruit seeds and their antibacterial activities with escherichia coli and salmonella bacteria.* Biocatalysis and Agricultural Biotechnology, 2019. **20**: p. 101241.
78. Kaviya, S., et al., *Biosynthesis of silver nanoparticles using citrus sinensis peel extract and its antibacterial activity.* Spectrochimica Acta Part A: Molecular and Biomolecular Spectroscopy, 2011. **79**(3): p. 594-598.
79. Masum, M.M.I., et al., *Biogenic Synthesis of Silver Nanoparticles Using Phyllanthus emblica Fruit Extract and Its Inhibitory Action Against the Pathogen Acidovorax oryzae Strain RS-2 of Rice Bacterial Brown Stripe.* Frontiers in Microbiology, 2019. **10**(820).
80. He, Y., et al., *Green synthesis of silver nanoparticles using seed extract of Alpinia katsumadai, and their antioxidant, cytotoxicity, and antibacterial activities.* RSC Advances, 2017. **7**(63): p. 39842-39851.
81. Özkar, S. and R.G. Finke, *Silver Nanoparticles Synthesized by Microwave Heating: A Kinetic and Mechanistic Re-Analysis and Re-Interpretation.* The Journal of Physical Chemistry C, 2017. **121**(49): p. 27643-27654.
82. Luty-Błocho, M., M. Wojnicki, and K. Fitzner, *Gold Nanoparticles Formation via Au(III) Complex Ions Reduction with l-Ascorbic Acid.* International Journal of Chemical Kinetics, 2017. **49**(11): p. 789-797.
83. Wojnicki, M., K. Fitzner, and M. Luty-Błocho, *Kinetic studies of nucleation and growth of palladium nanoparticles.* Journal of Colloid and Interface Science, 2016. **465**: p. 190-199.
84. Wagner, C., *Theorie der Alterung von Niederschlägen durch Umlösen (Ostwald-Reifung).* Zeitschrift für Elektrochemie, Berichte der Bunsengesellschaft für physikalische Chemie, 1961. **65**(7-8): p. 581-591.
85. Piwoński, I., et al., *Examination of Ostwald ripening in the photocatalytic growth of silver nanoparticles on titanium dioxide coatings.* Applied Surface Science, 2016. **373**: p. 38-44.
86. Shukla, D., A.A. Joshi, and A. Mehra, *Modeling of Formation of Nanoparticles in Reverse Micellar Systems: Ostwald Ripening of Silver Halide Particles.* Langmuir, 2009. **25**(6): p. 3786-3793.
87. Amirjani, A. and D.F. Haghshenas, *Modified Finke–Watzky mechanisms for the two-step nucleation and growth of silver nanoparticles.* Nanotechnology, 2018. **29**(50): p. 505602.
88. Ashley, B., et al., *Microwave Enhancement of Autocatalytic Growth of Nanometals.* ACS Nano, 2017. **11**(10): p. 9957-9967.

89. Kytsya, A., et al., *The Kinetic Rate Law for the Autocatalytic Growth of Citrate-Stabilized Silver Nanoparticles.* International Journal of Chemical Kinetics, 2015. **47**(6): p. 351-360.
90. Sandoe, H.E., M.A. Watzky, and S.A. Diaz, *Experimental probes of silver metal nanoparticle formation kinetics: Comparing indirect versus more direct methods.* International Journal of Chemical Kinetics, 2019. **51**(11): p. 861-871.
91. Harada, M., et al., *Characterization of water/AOT/benzene microemulsions during photoreduction to produce silver particles.* J Colloid Interface Sci, 2010. **343**(2): p. 423-32.
92. Tatarchuk, V.V., et al., *Kinetic Factors in the Synthesis of Silver Nanoparticles by Reduction of Ag+ with Hydrazine in Reverse Micelles of Triton N-42.* Chemistry of Materials, 2013. **25**(18): p. 3570-3579.
93. Calderón-Jiménez, B., et al., *Silver Nanoparticles: Technological Advances, Societal Impacts, and Metrological Challenges.* Frontiers in Chemistry, 2017. **5**(6).
94. Sobczak-Kupiec, A., et al. *Influence of silver nitrate concentration on the properties of silver nanoparticles*. Micro & Nano Letters, 2011. **6**, 656-660.
95. Demchenko, V., et al., *Effect of the type of reducing agents of silver ions in interpolyelectrolyte-metal complexes on the structure, morphology and properties of silver-containing nanocomposites.* Scientific Reports, 2020. **10**(1): p. 7126.
96. Skrabalak, S.E., et al., *On the Polyol Synthesis of Silver Nanostructures: Glycolaldehyde as a Reducing Agent.* Nano Letters, 2008. **8**(7): p. 2077-2081.
97. Mukherji, S., et al., *Synthesis and characterization of size- and shape-controlled silver nanoparticles.* Physical Sciences Reviews, 2019. **4**(1).
98. Liu, H., et al., *Effect of temperature on the size of biosynthesized silver nanoparticle: Deep insight into microscopic kinetics analysis.* Arabian Journal of Chemistry, 2020. **13**(1): p. 1011-1019.
99. Tang, T., et al., *Glass based micro total analysis systems: Materials, fabrication methods, and applications.* Sensors and Actuators B: Chemical, 2021. **339**: p. 129859.
100. Zhao, T., et al., *Size-controlled preparation of silver nanoparticles by a modified polyol method.* Colloids and Surfaces A: Physicochemical and Engineering Aspects, 2010. **366**(1): p. 197-202.
101. Feng, X., et al., *Synthetically Directed Self-Assembly and Enhanced Surface-Enhanced Raman Scattering Property of Twinned Crystalline Ag/Ag Homojunction Nanoparticles.* Langmuir, 2011. **27**(6): p. 2204-2210.
102. Alqadi, M.K., et al., *pH effect on the aggregation of silver nanoparticles synthesized by chemical reduction.* Materials Science-Poland, 2014. **32**(1): p. 107-111.
103. Marciniak, L., et al., *The Effect of pH on the Size of Silver Nanoparticles Obtained in the Reduction Reaction with Citric and Malic Acids.* Materials, 2020. **13**(23): p. 5444.
104. Qin, Y., et al., *Size control over spherical silver nanoparticles by ascorbic acid reduction.* Colloids and Surfaces A: Physicochemical and Engineering Aspects, 2010. **372**(1): p. 172-176.
105. Dong, X., et al., *Shape Control of Silver Nanoparticles by Stepwise Citrate Reduction.* The Journal of Physical Chemistry C, 2009. **113**(16): p. 6573-6576.
106. Ng, C.M., P.C. Chen, and S. Manickam, *Green High-Gravitational Synthesis of Silver Nanoparticles Using a Rotating Packed Bed Reactor (RPBR).* Industrial & Engineering Chemistry Research, 2012. **51**(15): p. 5375-5381.
107. Kisyelova, T., et al., *Effect of the reactor configuration on the production of silver nanoparticles*. 2016, AIDIC Servizi S.r.l. p. 121-126.
108. Roucoux, A., J. Schulz, and H. Patin, *Reduced Transition Metal Colloids: A Novel Family of Reusable Catalysts?* Chemical Reviews, 2002. **102**(10): p. 3757-3778.

109. Badawy, A.M.E., et al., *Impact of Environmental Conditions (pH, Ionic Strength, and Electrolyte Type) on the Surface Charge and Aggregation of Silver Nanoparticles Suspensions.* Environmental Science & Technology, 2010. **44**(4): p. 1260-1266.
110. Guerrini, L., R.A. Alvarez-Puebla, and N. Pazos-Perez, *Surface Modifications of Nanoparticles for Stability in Biological Fluids.* Materials, 2018. **11**(7).
111. Manojkumar, K., A. Sivaramakrishna, and K. Vijayakrishna, *A short review on stable metal nanoparticles using ionic liquids, supported ionic liquids, and poly(ionic liquids).* Journal of Nanoparticle Research, 2016. **18**(4): p. 103.
112. Tejamaya, M., et al., *Stability of Citrate, PVP, and PEG Coated Silver Nanoparticles in Ecotoxicology Media.* Environmental Science & Technology, 2012. **46**(13): p. 7011-7017.
113. Wang, M., et al., *Dispersibility and Size Control of Silver Nanoparticles with Anti-Algal Potential Based on Coupling Effects of Polyvinylpyrrolidone and Sodium Tripolyphosphate.* Nanomaterials (Basel), 2020. **10**(6).
114. Patel, K., et al., *Role of stabilizing agents in the formation of stable silver nanoparticles in aqueous solution: Characterization and stability study.* Journal of Dispersion Science and Technology, 2017. **38**(5): p. 626-631.
115. Izak-Nau, E., et al., *Impact of storage conditions and storage time on silver nanoparticles' physicochemical properties and implications for their biological effects.* RSC Advances, 2015. **5**(102): p. 84172-84185.
116. Pedregosa, F., et al., *Scikit-learn: Machine Learning in Python.* Journal of Machine Learning Research, 2011. **12**(85): p. 2825-2830.
117. Allen, M.P. and D.J. Tildesley, *Computer Simulation of Liquids: Second Edition*. 2 ed. 2017, Oxford: Oxford University Press. 640.
118. Andersson, B., et al., *Computational Fluid Dynamics for Engineers*. 2011, Cambridge: Cambridge University Press.
119. Marchisio, D.L., R.O. Fox, and R.O. Fox *Computational models for polydisperse particulate and multiphase systems*. Cambridge University Press, 2010. DOI: 10.1017/CBO9781139016599.
120. Tao, H., et al., *Nanoparticle synthesis assisted by machine learning.* Nature Reviews Materials, 2021. **6**(8): p. 701-716.
121. Furxhi, I., et al., *Practices and trends of machine learning application in nanotoxicology*, in *Nanomaterials*. 2020.
122. Shabanzadeh, P., et al., *Artificial intelligence in numerical modeling of silver nanoparticles prepared in montmorillonite interlayer space.* Journal of Chemistry, 2013.
123. shafaei, A. and G.R. Khayati, *A predictive model on size of silver nanoparticles prepared by green synthesis method using hybrid artificial neural network-particle swarm optimization algorithm.* Measurement, 2020. **151**: p. 107199.
124. Sattari, R. and G. Khayati, *Prediction of the size of silver nanoparticles prepared via green synthesis: A gene expression programming approach.* Scientia Iranica, 2020: p. 0-0.
125. Mekki-Berrada, F., et al., *Two-step machine learning enables optimized nanoparticle synthesis.* npj Computational Materials, 2021. **7**(1): p. 55.
126. Sun, B., M. Fernandez, and A.S. Barnard, *Machine Learning for Silver Nanoparticle Electron Transfer Property Prediction.* Journal of Chemical Information and Modeling, 2017. **57**(10): p. 2413-2423.
127. Hashemnia, S., et al., *An investigation of the effect of PVP-coated silver nanoparticles on the interaction between clonazepam and bovine serum albumin based on*

molecular dynamics simulations and molecular docking. Journal of Molecular Liquids, 2021.
128. Hazarika, Z. and A.N. Jha, *Computational Analysis of the Silver Nanoparticle-Human Serum Albumin Complex.* ACS Omega, 2020.
129. Luo, W., W. Hu, and S. Xiao, *Size Effect on the Thermodynamic Properties of Silver Nanoparticles.* The Journal of Physical Chemistry C, 2008. **112**: p. 2359-2369.
130. Yoneya, M. and S.Y. Sugisawa, *Simulation of Colloidal Silver Nanoparticle Formation from a Precursor Complex.* Journal of Physical Chemistry C, 2019.
131. Meneghetti, M.R., C.M. Soares, and J.A. Da Silva, *Molecular dynamics simulations suggest a possible role for no in the polyol synthesis of silver nanostructures.* Journal of Physical Chemistry C, 2020.
132. Tsuji, M., et al., *Effects of chain length of polyvinylpyrrolidone for the synthesis of silver nanostructures by a microwave-polyol method.* Materials Letters, 2006.
133. Mdluli, P.S., et al., *Selective adsorption of PVP on the surface of silver nanoparticles: A molecular dynamics study.* Journal of Molecular Structure, 2011.
134. Qi, X., et al., *How Structure-Directing Agents Control Nanocrystal Shape: Polyvinylpyrrolidone-Mediated Growth of Ag Nanocubes.* Nano Letters, 2015.
135. Kyrychenko, A., et al., *Atomistic Simulations of Coating of Silver Nanoparticles with Poly(vinylpyrrolidone) Oligomers: Effect of Oligomer Chain Length.* The Journal of Physical Chemistry C, 2015. **119**: p. 7888-7899.
136. Balankura, T., et al., *Oriented attachment mechanism of triangular Ag nanoplates: A molecular dynamics study.* Nanoscale Advances, 2020.
137. Balbuena, C., M.M. Gianetti, and E.R. Soulé, *Molecular dynamics simulations of the formation of Ag nanoparticles assisted by PVP.* Physical Chemistry Chemical Physics, 2021.
138. Zeng, Q., et al., *Growth mechanisms of silver nanoparticles: a molecular dynamics study.* Nanotechnology, 2007. **18**: p. 035708.
139. Yang, C., et al., *Molecular dynamics simulation of a positively charged silver nanoparticle capped by cetyltrimethylammonium cations.* Colloids and Surfaces A: Physicochemical and Engineering Aspects, 2006.
140. Kyrychenko, A., D.A. Pasko, and O.N. Kalugin, *Poly(vinyl alcohol) as a water protecting agent for silver nanoparticles: the role of polymer size and structure.* Physical Chemistry Chemical Physics, 2017. **19**: p. 8742-8756.
141. Milek, T. and D. Zahn, *Molecular simulation of Ag nanoparticle nucleation from solution: Redox-reactions direct the evolution of shape and structure.* Nano Letters, 2014.
142. Liu, H., et al., *Modeling of Silver Nanoparticle Formation in a Microreactor: Reaction Kinetics Coupled with Population Balance Model and Fluid Dynamics.* Industrial & Engineering Chemistry Research, 2014. **53**: p. 4263-4270.
143. Zhou, Y., et al., *Quantitative nucleation and growth kinetics of gold nanoparticles via model-assisted dynamic spectroscopic approach.* Journal of Colloid and Interface Science, 2013.
144. Yuan, C., *Quadrature-based moment methods for polydisperse multiphase flow modeling Recommended Citation*. 2013. p. 1 - 16.
145. Madadelahi, M. and A. Shamloo, *Droplet-based flows in serpentine microchannels: Chemical reactions and secondary flows.* International Journal of Multiphase Flow, 2017.
146. Liu, H., et al., *Continuous biosynthesis of silver nanoparticles in a hydrodynamic cavitation device and modeling of the process by numerical simulation strategy.* Journal of Nanoparticle Research, 2018.

147. Badilescu, S. and M. Packirisamy, *Microfluidics-Nano-Integration for Synthesis and Sensing.* Polymers, 2012. **4**(2): p. 1278-1310.
148. Baber, R., et al., *An engineering approach to synthesis of gold and silver nanoparticles by controlling hydrodynamics and mixing based on a coaxial flow reactor.* Nanoscale, 2017. **9**(37): p. 14149-14161.
149. Makgwane, P.R. and S.S. Ray, *Synthesis of nanomaterials by continuous-flow microfluidics: a review.* J Nanosci Nanotechnol, 2014. **14**(2): p. 1338-63.
150. Shembekar, N., et al., *Droplet-based microfluidics in drug discovery, transcriptomics and high-throughput molecular genetics.* Lab on a Chip, 2016. **16**(8): p. 1314-1331.
151. Wu, K.J., G.M. De Varine Bohan, and L. Torrente-Murciano, *Synthesis of narrow sized silver nanoparticles in the absence of capping ligands in helical microreactors*, in *Reaction Chemistry and Engineering*. 2017.
152. Shen, F., et al., *Advances in Micro-Droplets Coalescence Using Microfluidics.* Chinese Journal of Analytical Chemistry, 2015. **43**: p. 1942-1954.
153. Seemann, R., et al., *Droplet based microfluidics.* Rep Prog Phys, 2012. **75**(1): p. 016601.
154. Anna, S.L., *Droplets and Bubbles in Microfluidic Devices.* Annual Review of Fluid Mechanics, 2016. **48**(1): p. 285-309.
155. Kovalchuk, N.M., et al., *Effect of surfactant on emulsification in microchannels.* Chemical Engineering Science, 2018. **176**: p. 139-152.
156. Li, X.B., et al., *Study on the mechanism of droplet formation in T-junction microchannel.* Chemical Engineering Science, 2012.
157. Sivasamy, J., et al., *An investigation on the mechanism of droplet formation in a microfluidic T-junction.* Microfluidics and Nanofluidics, 2011.
158. Wojnicki, M., et al., *Continuous, monodisperse silver nanoparticles synthesis using microdroplets as a reactor.* Journal of Flow Chemistry, 2019. **9**(1): p. 1-7.
159. Kašpar, O., et al., *Governing factors for preparation of silver nanoparticles using droplet-based microfluidic device.* Biomedical Microdevices, 2019. **21**(4): p. 88.
160. Lin, X.Z., A.D. Terepka, and H. Yang, *Synthesis of Silver Nanoparticles in a Continuous Flow Tubular Microreactor.* Nano Letters, 2004. **4**(11): p. 2227-2232.
161. Baber, R., et al., *Synthesis of silver nanoparticles in a microfluidic coaxial flow reactor.* RSC Advances, 2015. **5**(116): p. 95585-95591.
162. Lazarus, L.L., et al., *Two-Phase Microfluidic Droplet Flows of Ionic Liquids for the Synthesis of Gold and Silver Nanoparticles.* ACS Applied Materials & Interfaces, 2012. **4**(6): p. 3077-3083.
163. Liu, G., et al., *Controllable Synthesis of Silver Nanoparticles Using Three-Phase Flow Pulsating Mixing Microfluidic Chip.* Advances in Materials Science and Engineering, 2018. **2018**: p. 14.
164. Xu, L., et al., *Droplet synthesis of silver nanoparticles by a microfluidic device.* Chemical Engineering and Processing: Process Intensification, 2016. **102**: p. 186-193.
165. Kovalchuk, N.M., et al., *Drop formation in microfluidic cross-junction: jetting to dripping to jetting transition.* Microfluidics and Nanofluidics, 2019. **23**(8).
166. Kahouadji, L., et al., *Simulation of immiscible liquid–liquid flows in complex microchannel geometries using a front-tracking scheme.* Microfluidics and Nanofluidics, 2018. **22**: p. 126.
167. Soh, G.Y., G.H. Yeoh, and V. Timchenko, *Numerical investigation on the velocity fields during droplet formation in a microfluidic T-junction.* Chemical Engineering Science, 2016.
168. Garstecki, P., et al., *Formation of droplets and bubbles in a microfluidic T-junction - Scaling and mechanism of break-up.* Lab on a Chip, 2006.

169. Filimonov, R., Z. Wu, and B. Sundén, *Toward computationally effective modeling and simulation of droplet formation in microchannel junctions.* Chemical Engineering Research and Design, 2021.
170. Wu, Z., Z. Cao, and B. Sundén, *Liquid-liquid flow patterns and slug hydrodynamics in square microchannels of cross-shaped junctions.* Chemical Engineering Science, 2017.
171. Wu, L., et al., *Role of local geometry on droplet formation in axisymmetric microfluidics.* Chemical Engineering Science, 2017. **163**: p. 56-67.
172. Chinaud, M., E.P. Roumpea, and P. Angeli, *Studies of plug formation in microchannel liquid-liquid flows using advanced particle image velocimetry techniques.* Experimental Thermal and Fluid Science, 2015.
173. Kašpar, O., et al., *Governing factors for preparation of silver nanoparticles using droplet-based microfluidic device.* Biomedical Microdevices, 2019.
174. Wang, J., et al., *Fluid mixing in droplet-based microfluidics with a serpentine microchannel.* RSC Advances, 2015.
175. Sarrazin, F., et al., *Experimental and numerical study of droplets hydrodynamics in MicroChannel.* AIChE Journal, 2006.
176. Song, H., J.D. Tice, and R.F. Ismagilov, *A Microfluidic System for Controlling Reaction Networks in Time.* Angewandte Chemie International Edition, 2003. **42**(7): p. 768-772.
177. Wu, K.J., G.M. De Varine Bohan, and L. Torrente-Murciano, *Synthesis of narrow sized silver nanoparticles in the absence of capping ligands in helical microreactors.* Reaction Chemistry and Engineering, 2017.
178. Kovalchuk, N.M., et al., *Mass Transfer Accompanying Coalescence of Surfactant-Laden and Surfactant-Free Drop in a Microfluidic Channel.* Langmuir, 2019. **35**(28): p. 9184-9193.
179. Tung, K.Y., C.C. Li, and J.T. Yang, *Mixing and hydrodynamic analysis of a droplet in a planar serpentine micromixer.* Microfluidics and Nanofluidics, 2009.
180. Muradoglu, M. and H.A. Stone, *Mixing in a drop moving through a serpentine channel: A computational study.* Physics of Fluids, 2005.
181. CHANDORKAR, A. and S. PALIT, *Simulation of Droplet Dynamics and Mixing in Microfluidic Devices Using a VOF-Based Method.* Sensors & Transducers, 2009: p. 136-149.
182. Özkan, A. and E.Y. Erdem, *Numerical analysis of mixing performance in sinusoidal microchannels based on particle motion in droplets.* Microfluidics and Nanofluidics, 2015.
183. Filatov, N.A., et al., *The study of mixing of reagents within a droplet in various designs of microfluidic chip*, in *Journal of Physics: Conference Series*. 2016.
184. Yang, L., et al., *Fluid mixing in droplet-based microfluidics with T junction and convergent-divergent sinusoidal microchannels.* ELECTROPHORESIS, 2018. **39**: p. 512-520.